An Infrared Stellar Thermometer: Exploiting IGRINS Spectra

Emelie Sandved

Lund Observatory
Lund University

2022-EXA190

Degree project of 15 higher education credits
June 2022

Supervisor: Nils Ryde
Co-supervisor: Govind Nandakumar

Lund Observatory
Box 43
SE-221 00 Lund
Sweden

Abstract

Using the infrared (IR) spectral range when measuring stellar spectra is beneficial compared to using the optical range mainly when observing distant stars through the dust dense interstellar regions in the Galactic mid-plane. Methods to determine stellar parameters from IR spectra are, however, not fully developed yet because technological difficulties in creating reliable IR detectors have slowed the advance of such methods.

The effective temperature of a star is considered to be one of the most fundamental parameters of a star because it is used in stellar classifications and also because it is directly related to the star's energy output, which furthermore affects the formation of spectral lines. Therefore, it is important for astronomers to be able to determine accurate stellar temperatures.

This thesis aims to investigate whether OH and CO molecular lines from IR spectra in the H-band ($15,000$ - $18,000\,\text{Å}$) can be used to determine the effective temperature of stars. These lines' sensitivity to the stellar surface gravity, oxygen abundance, and for the CO lines, the carbon abundance were explored as well.

There already exist many methods to determine the effective temperature of stars, but the majority of these use optical spectra instead of IR. In this thesis, spectral synthesis is used to determine the temperatures of 34 K-giants. Their spectra were observed with the near-IR, high-resolution spectrometer, IGRINS mounted on the 4.3 m Lowell Discovery Telescope in Flagstaff, Arizona. The stellar temperatures that are determined in this thesis are benchmarked against optically determined temperatures from Jönsson et al. (in prep). Other stellar parameters that were assumed in the spectral synthesis, such as the surface gravity, the oxygen abundance and the carbon abundance, were also taken from Jönsson et al. (in prep).

The results found in this thesis show that OH lines provide accurate temperatures within $|100|$ K and that they are insensitive to the surface gravity (1 K/0.2 dex) but very sensitive to the oxygen abundance (120 K/0.2 dex). It was further found that the CO lines were sensitive to the surface gravity (100 K/0.2 dex) and the carbon abundance (320 K/0.2 dex for cooler stars and 220 K/0.2 dex for hotter stars), but less sensitive to the oxygen abundance (20 K/0.2 dex). A combination of the CO and OH lines showed that the sensitivities decreased compared to the most sensitive linelist (-13 K/0.2 dex for the surface gravity and 100 K/0.2 dex for the oxygen abundance). The combination also acquired properties from both linelists such as their sensitivities and estimated temperatures that lie in between the temperatures determined from the separate linelists.

Acknowledgements

I would like to thank both my supervisor Nils Ryde and my co-supervisor Govind Nandakumar for all the help and support during my thesis project. I would also like to thank Brian Thorsbro and Rebecca Forsberg for their help as well in my project. Without all of their help, I would not have been able to write this thesis.

Populärvetenskaplig beskrivning

Genom att analysera stjärnors egenskaper, kan astronomer ta reda på hur både stjärnor och galaxer utvecklas och formas. Det främsta verktyget man använder till detta är så kallade spektra. När vitt ljus, från exempelvis en lampa, färdas genom ett prisma så ser man regnbågens färger på andra sidan prismat. Detta kallas för ett spektrum. När ljus exempelvis färdas genom ett moln, innan det delas upp till ett spektrum, så får man svarta streck i spektrat där ljus saknas. Dessa kallas absorptionslinjer som motsvarar ljusabsoprtion av speciella atomer och molekyler. På det viset så kan man se vad molnet innehåller genom att titta på dess spektrum.

I stället för att använda ett prisma så använder astronomer ofta instrument som man kallar för spektrografer som delar upp ljuset till ett spektrum, som också kan överföra spektrat till en dator. I de spektrumen så kan man mäta mer än det synliga ljuset, det man ser med blotta ögat, utan man kan också mäta våglängder som vi människor inte kan se. Om ljuset innehåller mer energi så är ljuset blåare och kallas för ultraviolett- (UV), röntgen- och gamma-strålning, men om ljuset innehåller mindre energi så är det rödare och kallas för infraröd- (IR), mikro- och radio-strålning.

Fördelen med att jobba i infrarött är att det inte blir hindrat av moln och gas som synligt ljus blir. Det gör att man kan observera stjärnor som annars är gömda bakom gas och stoft i rymden om man observerar i IR. Däremot så är IR spektroskopi inte lika utvecklad som spektroskopi med synligt ljus på grund av teknologiska svårigheter. Det betyder att tekniker till att analysera IR spektra inte är lika utvecklade och därför behöver det undersökas vad som fungerar och inte.

De viktigaste egenskaperna hos stjärnor är deras temperatur, deras ytgravitation och deras mängd metaller, som här betyder alla ämnen som är tyngre än väte och helium. Mitt arbete syftar till att hitta metoder som kan användas till att bestämma stjärnors temperatur genom att analysera deras spektra i infrarött. Denna rapport undersöker om OH och CO molekyler i jättar kan användas till detta syfte och vilka svagheter de har. Exempelvis, hur känsliga spektrallinjerna är för ytgravitationen, mängden syre (O) eller mängden kol (C) i stjärnan.

Mätningarna visar att OH linjer är relativt okänsliga för ytgravitationen men betydligt mer känsliga för syremängden. CO linjerna visar däremot en motsatt effekt, där de är väldigt känsliga för ytgravitationen men inte speciellt känsliga för syrehalten. De är också väldigt känsliga för mängden kol. Om man kombinerar linjerna i mätningarna så får resultatet effekter från båda uppsättningarna linjer. De blir därför påverkade av både positiva och negativa egenskaper hos linjerna, som deras känsligheter. Därför kommer astronomer behöva ta linjernas egenskaper i beaktning om de ska användas i framtida studier så att linjerna som väljs ger bästa möjliga resultat.

Contents

List of Figures

List of Tables

Chapter 1

Introduction

Stellar spectra are used to determine important stellar parameters such as effective temperature, surface gravity and chemical composition (Gray, 2021). Knowing these quantities can in turn teach astronomers about stellar evolution, the evolution of stellar populations as well as galaxy evolution. For example, stellar parameters are important to estimate abundances of age-indicating elements like iron, α elements (e.g. Mg), Y, etc. , to divide stars in the Milky Way into different stellar populations with different ages. This way, reliable estimation of stellar parameters from stellar spectra plays a crucial role in teaching us about various formation scenarios of the Milky Way, which can teach us about the formation and evolution of galaxies similar to the Milky Way. Therefore, it is important to be able to analyse stellar spectra to learn more about our universe as a whole.

In stellar spectra, various wavelength regions can show different parts of the star. For example, ultraviolet (UV) and x-ray wavelengths ($< 4000\,\text{Å}$) can show parts of the stellar chromosphere and corona, whereas the optical region (approximately 4000 to $7000\,\text{Å}$) can show parts of the stellar photosphere (Gray, 2021). Accordingly, each wavelength region has developed into separate research areas such as radio- or UV-astronomy.

However, the techniques for spectral analysis in the near-infrared (NIR) to mid-infrared (approximately $10,000$ to beyond $100,000\,\text{Å}$) are not fully developed due to mainly technological reasons (Rieke, 2009). The goal of this thesis is to investigate if we can use spectral lines in the H-band ($15,000$ - $18,000\,\text{Å}$) from the diatomic CO and OH molecules to determine the effective temperature of K-giants (red giants of spectral class K, ~ 4000 - $5000\,\text{K}$). Their sensitivities to the surface gravity, to the oxygen abundance and the carbon abundance (for CO lines) are investigated as well. This way, astronomers can know how accurate the surface gravity, the oxygen abundance and the carbon abundance have to be in order to determine accurate temperatures using these spectral lines.

The majority of chapter 1 aims to cover the most important concepts needed to understand the content of this thesis. It includes an introduction to infrared spectroscopy explaining both its advantages and disadvantages, information about important stellar parameters, spectral line formation and commonly used methods to determine both the effective temperature and the surface gravity. Then follows chapter 2 where the method is explained after which the results are presented and discussed in chapter 3. A conclusion in chapter 4 then summarizes the most important points in this thesis.

1.1 Infrared spectroscopy

There are many advantages to study spectra in the infrared (IR) wavelengths instead of the optical. The main benefit is that IR radiation does not interact as much with matter as optical radiation does. This is because IR light, which has longer wavelengths than optical light, is much less likely to get scattered by matter and consequently, it does not get obscured by interstellar clouds. Therefore, when observing in optical wavelengths, stars near our Galaxy's centre are obscured by interstellar dust clouds and can hence be difficult to observe. It is also more sensitive to so-called reddening, which is when the light from e.g. a star becomes redder as the shorter wavelengths are scattered more by the dust whereas the red light gets through more easily. This is not a problem when observing in the IR, which makes it possible to still investigate these stars despite the physical hindrances.

Another benefit is that cooler stars, in particular red giants, are among the brightest stars in the IR spectral range. Accordingly, these stars can be seen at greater distances than hotter dwarf stars, which allows astronomers to map dust-dense regions in space that would otherwise be obscured when observing using optical instruments. Additionally, for stars cooler than approximately 6000 K, molecules can begin to form in the atmosphere (Masseron, 2015), whose absorption lines can be observed in stellar spectra. However, if the stars are too cool, less than approximately 4000 K, the abundance of molecules increase such that molecular lines dominate, in particular in optical spectra, making it hard to distinguish separate spectral lines and thereby making the analysis of the spectra close to impossible. Examples of problems arising are line blending and difficulty to identify the continuum in optical spectra (Jönsson et al., 2017), mainly due to TiO (titanium oxide). Note, however, that this is less of a problem in IR spectra since TiO lines only lie in the optical region. In the near-IR CN, CO and OH are the most common molecules, where CO and OH molecules are examples of temperature sensitive molecules. When stellar temperatures rise above approximately 5000 K, these molecules dissociate and can no longer form as the energy is too high. In Smith et al. (2013), they show that CO and OH lines are clearly visible at lower temperatures, but they start to fade in the spectrum of µLeo ($T_{\mathrm{eff}} \approx 4500\,\mathrm{K}$; K2 IIIb), where the temperature is close to too hot to contain them. Therefore, these molecules can only be observed in K-type or cooler giant stars. Whereas for dwarf stars, where the surface gravity is larger, they can be observed for higher temperatures.

However, IR spectroscopic analysis methods are not fully developed, mainly due to technological difficulties when creating reliable infrared detectors. The main issues for ground-based telescopes operating in the IR are the heat-noise from the atmosphere and the surrounding environment as there are many heat-sources creating false signals in the detectors (Storey, 2000). Therefore, they often have to be cooled down, to eliminate this problem. Initially this made IR detectors incompatible to charge couple devices (CCDs), as they cannot operate at such low temperatures without creating a lot of noise. This was, however, overcome by adding so-called "readout amplifiers", which were placed behind each pixel in the CCDs to amplify the signals (Rieke, 2009).

Before IR detectors were built for astronomy research purposes they were often built for military purposes after which they were integrated into IR astrophysics spectroscopy. They are built in different materials: being indium antimony (InSb), mercury cadmium telluride (HgCdTe) and silicon (Si) (Rieke, 2009). Silicon CCDs are among the best detectors for near-IR astrophysics and are thus the most commonly used detectors for this purpose (Watkins et al., 2020).

The Immersion GRating INfrared Spectrograph (IGRINS), which was used to measure the spectra of this thesis' stellar sample, uses a silicon immersion grating and two HgCdTe detectors. It can measure spectra in both the H- and the K-band (2.2 µm). It is a so-called high-resolution spectrograph with a resolution of $R = 40,000$ (Yuk et al., 2010).

Telescopes operating in the IR are still being developed. For example, the newly launched James Webb Space Telescope (JWST) is equipped with detectors that are able to detect IR wavelengths, albeit at lower spectral resolutions (Rieke, 2009). Reliable and efficient methods of analysis of IR spectra are required to be able to properly investigate them and extract all available information.

1.2 Stellar parameters

To properly characterize a star, several parameters are used; the most important being the effective temperature, the surface gravity and the metallicity. These can tell us much about the properties of a star but they can be difficult to determine. In the following three sections, the most important stellar properties for this thesis, the effective temperature, the surface gravity and the molecular abundances are defined and explained.

To begin with, the temperature of a star is not uniform. For example, in our Sun the temperatures in the outer layers are 4000-5000 K, whereas further out in the chromosphere and in the corona, the temperatures can reach 3 orders of magnitude larger. The radius of a star is not well-defined either as it is defined by the place in the star from which the light can escape. This region is the innermost part of the star's atmosphere, called the photosphere. Most of the visible light comes from this region and the majority of the spectral lines are formed in there as well. A star's atmosphere is defined as the transition region between the stellar interior and the interstellar medium (Gray, 2021).

In the innermost part of the photosphere, the temperature is very high and energy transfer through collisions dominate. The temperature then decreases further out in the photosphere and the domination of collisions decreases with the temperature. Below the photosphere, the gas of the star is optically thick, such that the light cannot escape before it is scattered. Therefore, the photosphere is the first region of a star that is optically thin enough for the light to be able to escape out from the star. This creates a visual surface that can be seen when observing the Sun. The parts of the stellar atmosphere following the photosphere are the chromosphere and the corona, where the corona is the outermost part of the atmosphere. The temperature increases in these regions and the majority of the radiation from these regions is seen in the UV wavelength range (Gray, 2021).

1.2.1 Effective temperature

One of the properties that astronomers use to characterize stars is the effective temperature, T_{eff}. As was mentioned before, the temperature is not uniform throughout the layers of a star and must therefore be defined in another way that is easier to measure. It is thus defined as the temperature corresponding to the total power output per unit area radiated from the star,

$$\int\limits_0^\infty \mathfrak{F}_\nu \mathrm{d}\nu \equiv \sigma T_{\text{eff}}^4, \tag{1.1}$$

where $\sigma = 5.6704 \cdot 10^{-5}\,\mathrm{erg\,s^{-1}\,cm^{-2}\,K^{-4}}$ is the Stefan-Boltzmann constant and where the integral of flux over frequency (defined as bolometric flux), gives the total radiated power per unit area (Gray, 2021). Equation 1.1 has the same form as the Stefan-Boltzmann law, which means that the total power output from a star with effective temperature T_{eff} is the same as that of a black-body radiator with the same temperature. This is further related to the luminosity, L, of a star, which is the total power emitted by the star. The relation is as follows,

$$L = 4\pi R^2 \int\limits_0^\infty \mathfrak{F}_\nu \mathrm{d}\nu = 4\pi R^2 \sigma T_{\text{eff}}^4, \tag{1.2}$$

where R is the radius of the star.

The effective temperature is used when classifying different types of stars. They are denoted from the hottest to the coldest stars with the letter sequence: O, B, A, F, G, K, M. These have further sub-classifications with numbers as there are very many types of stars and since its initiation, the sequence has been further extended (Gray, 2021). Most spectral lines have certain temperature intervals where they are the most apparent. The temperature determines the dominating chemical populations in the star, and hence also the abundances. In a cool star, molecules dominate the populations and in a hot star, ionized elements dominate the populations.

Both the luminosity and the effective temperature are plotted against each other to create what is called the Hertzsprung-Russel diagram (HR-diagram). An example of such a diagram can be seen in Figure 1.1. With this diagram, stars can be divided into further sub-categories such as main-sequence stars, giants and supergiants. Our Sun, for example, is a main-sequence star. Through this diagram, different stellar evolutions can be easily mapped.

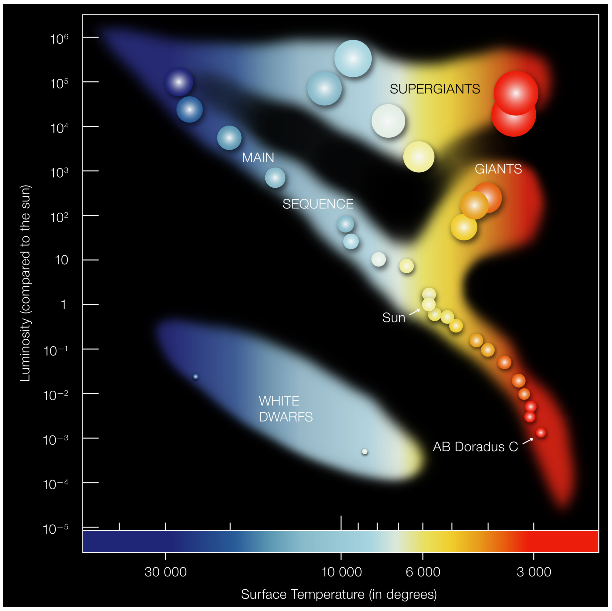

Figure 1.1: This figure shows an example of the so-called HR-diagram. On the y-axis in the diagram is the luminosity plotted compared to the Sun and on the x-axis is the surface temperature plotted in [K]. Because the luminosity is normalized to the Sun, the Sun can be seen on the main sequence where the luminosity equals 1. Typical stellar colours are shown in the diagram, presenting stellar evolutionary tracks. The main sequence together with giants, super-giants and white dwarfs are marked in the diagram as well. (Source: ESO)

1.2.2 Surface gravity

The second important property of stars is the surface gravity. It is defined through Newton's gravitational law,

$$g = G\frac{M}{R^2}, \tag{1.3}$$

where M is the mass of the star, R is the radius of the star and $G = 6.67259 \cdot 10^{-8}\,\mathrm{cm}^3\,\mathrm{g}^{-1}\,\mathrm{s}^{-2}$ is the gravitational constant. The typical unit for the surface gravity is $\mathrm{cm\,s}^{-2}$. It is often customary to use $\log g$ when discussing the surface gravity of a star. In this case the 'unit' used is dex, which stands for "decimal exponent". For example, 2 dex corresponds to $100\,\mathrm{cm\,s}^{-2}$ and -1 dex to $0.1\,\mathrm{cm\,s}^{-2}$. With the mass of the star known and the surface gravity measured, the radius of the star can be determined. Methods used to determine the surface gravity are discussed in oncoming sections.

The surface gravity is important because it affects the pressure within the stars' atmospheres, which affects the interactions that create the spectra and the spectral lines. The level of ionization of the elements within the atmosphere depends on the pressure, which means that the extinction coefficients for both the spectral lines and the continuum are dependent on the pressure and hence the surface gravity as well.

1.2.3 Molecular abundances

Molecular abundances are largely dependent on the atomic abundances of the atoms that the molecules consist of. The abundances of atoms in stars are given as the number density, N_X, of the element of interest compared to the number density of hydrogen, N_H, in the star. In that way, the amount of atoms of a certain element is given per hydrogen atom. Because hydrogen is vastly more abundant than any other element in stars, the result from the comparison is always very small. To solve this, the logarithm of the abundance is often calculated instead, giving a 'unit' of dex. When talking about abundances of atoms in stars, astronomers often define them in comparison to the solar abundance of the same element, therefore the abundance given for a certain element, X, in a star is calculated as

$$[X/\mathrm{H}] = log\left(\frac{N_X}{N_\mathrm{H}}\right)_\star - log\left(\frac{N_X}{N_\mathrm{H}}\right)_\odot, \tag{1.4}$$

where the bracket notation signals that the abundance is relative to the solar abundances. The number density of the element is obtained using the Saha distribution and the Boltzmann distribution. The Saha distribution gives the ratio of the number density of the element in a particular ionization state, N_{r+1}, compared either to the number density of all other ionization states, N, or to the number density of the element in the lower ionization state, N_r, hence N_{r+1}/N or N_{r+1}/N_r. The Boltzmann distribution compares the number densities of different excitation states, s and t, of an element in a certain ionization stage, r, hence $n_{r,s}/n_{r,t}$. Together, these can provide the total number density of the element such that it can be used in Equation 1.4 (Gray, 2021).

In many cases it is interesting to compare the content of different stars to each other. This can, for example, allow astronomers to see if any of the stars stand out compared to stars with similar properties (e.g. stars with similar metallicity can have different elemental abundances). Then it is often more beneficial to calculate the elemental abundance compared to the metallicity (i.e. calculate $[X/\mathrm{Fe}]$ for some element X), instead of calculating the elemental abundance compared to the hydrogen abundance. It is calculated similarly as in Equation 1.4, but with the iron abundance in the denominator instead of the hydrogen abundance.

When calculating molecular abundances, every place where the constituent atoms might be other than the molecule of interest has to be taken into account in a so-called chemical or molecular equilibrium. For example, in OH molecules the possible presence of oxygen in CO, CO_2, H_2O, free oxygen, etc. , must be taken into account. The same goes for the hydrogen present in the OH molecule. Thus, the total abundance of an element, X, in a stellar atmosphere is given by the ratio between the so-called fictional partial pressure from the desired element if all molecules containing this element were dissociated and the fictional partial pressure if all types of molecules were dissociated. However, this cannot be directly measured and hence this is instead calculated through (Short & Bennett, 2021),

$$\alpha_k = \frac{\sum_n N_{nk} p_n}{\sum_n N_n p_n}, \tag{1.5}$$

where k is the desired element (e.g. oxygen), N_{nk} is the number of atoms of element k in molecule n (e.g. for the OH molecule and element O, $N_{\mathrm{OH,O}} = 1$), N_n is the number of atoms in molecule n (e.g. for the OH molecule, $N_{\mathrm{OH}} = 2$) and p_n is the total partial pressure from all molecules n. Since it is a sum over all molecules n containing the element k, all possible places where the element can occur is taken into account. The values in the fraction are taken from the molecular equilibrium constant K_n of a molecule n. K_n is the ratio between the product of the partial pressures of the atoms making up the molecule and the partial pressure from the molecule (Short & Bennett, 2021). For example, for OH the partial pressure for the molecule is denoted p_{OH}, where p_{O} and p_{H} are the partial pressures for the atoms in OH. This gives the molecular equilibrium constant,

$$K_{\mathrm{OH}} = \frac{p_{\mathrm{O}} p_{\mathrm{H}}}{p_{\mathrm{OH}}}.$$

1.3 Spectral line formation

To be able to interpret the information found in spectra, it is essential to understand how spectral lines are formed in stellar atmospheres. In the following sections, it is described how spectral lines from molecules are formed and which lines are best to target for spectral analysis.

1.3.1 Molecular transitions and bandheads

In molecules, there are three main types of transitions that create spectral lines: electronic, vibrational and rotational transitions. Electronic transitions are caused by excited electrons in the atoms that make up the molecule. These transitions mainly affect the binding of the atoms within the molecule, which gets weaker for higher excitation levels. It also weakens the energy levels of the other types of transitions. The electronic energy levels are often denoted by n. Vibrational transitions are different vibrational states in the atoms of the molecule. These are often compared to the harmonic oscillator of two masses fastened to each other by a spring. Molecules always have a small vibration, which means that the vibrational energy state is never equal to zero. However, it has a ground-state vibration with a specific frequency (often labeled ν_0). The vibrational states create sub-levels in between the different electronic energy levels. The vibrational energy levels are often denoted by ν. Lastly, the rotational transitions are different rotational states where the whole molecule rotates around its own axis. These create sub-levels for the vibrational energy states. The rotational energy levels are often denoted by J (Buyana, 1997).

For molecules, the vibrational and rotational energy transitions are coupled to each other and are often together called vibrational-rotational or ro-vibrational energy transitions. One does not happen without the other. Nonetheless, pure vibrational and pure rotational transitions can occur. Ro-vibrational transitions create spectral lines in the IR spectral region, and are hence important for the purpose of this thesis. This fine-structure of the energy levels, create many spectral lines in close proximity in the spectra. These are called spectral bands and with a high resolution spectrograph, the separate spectral lines can be distinguished (Buyana, 1997).

The fine-structure can be divided into three main branches with spectral lines: the P-, R- and Q-branch. These are groupings of spectral lines that have the same ΔJ. They often spread out over several frequencies, due to slightly different rotational constants of the upper and lower levels. Eventually, the trend of the spectral lines within the branches turn, which causes the bands to fold upon themselves, from which, several spectral lines are gathered in a smaller frequency interval at the turning point. These gatherings are called molecular bandheads, which are beneficial to use in spectral analysis of stars since they present many lines (Buyana, 1997).

In theory, diatomic molecules can be approximated as harmonic oscillators, with a limitation to only allow vibrational energy transitions of $\Delta\nu = \pm1$. However, in reality the difference between vibrational energy levels in the transitions can be $\Delta\nu = \pm1$, ±2, ±3 and higher (Buyana, 1997). In this thesis, only ±2 and ±3 are encountered.

1.3.2 Weak Line Approximation

When measuring spectra from stars, one will notice that the spectral lines have different depths and different widths. These properties are together defined as the strength of the spectral lines, where deep lines are strong, and shallow lines are weak. Different types of spectral lines are beneficial to use for different purposes. For the determination of abundances, which is essential for this thesis, weak lines are the most reliable lines to use. For weak lines, the logarithm of the abundance is linearly related to the logarithm of the line strength, hence giving accurate abundances if the line strength is measured. The line strength is measured by the equivalent width, which is a rectangle of height 1 and width equal to the area of the spectral line. For weak lines, the strength of the lines are almost entirely dependent on the abundance. This approximation is called the weak-line approximation (Gray, 2021).

Strong lines are very sensitive to the micro-turbulence, which makes strong lines unreliable for determining the abundance. Strong lines are better to use to determine the pressure and the surface gravity in stars since the line wings are sensitive to these parameters (Gray, 2021).

1.4 Methods for determining T_{eff}

As was stated before, the effective temperature of a star is very important as it is directly related to the energy distribution and energy output of the star. It is considered a fundamental stellar parameter because it directly affects the determination of elemental abundances in spectral analysis. Therefore, astronomers use several different methods to determine the effective temperature as accurately as possible. The most commonly used methods to determine the effective temperature are presented in this section, giving an understanding of how they work together with both their advantages and their disadvantages.

1.4.1 Infrared Flux Method (IRFM)

The infrared flux method was first presented by Blackwell & Shallis (1977) and it was the first method for determining the effective temperature without large dependency on model stellar atmospheres. This was highly desired by astronomers as different models could potentially generate very different effective temperatures for the same data (Casagrande et al., 2010).

The photosphere is the part of a star from which the majority of the absorption lines are created, as was described earlier. In FGK-type stars, the absorption is very small in the IR region ($> 7000\,\text{Å}$), which makes it possible to approximate the flux from the star in IR with the Rayleigh-Jeans approximation of a black-body (Jofré et al., 2019; Casagrande et al., 2010).

In the IRFM the quotient between the bolometric flux, F_{bol}, and the monochromatic flux at a certain IR wavelength, $F_{\lambda_{\text{IR}}}$, is calculated for both the fluxes measured at the surface of the Earth with different photometric colour filters (Casagrande et al., 2006), giving the observational R-factor, R_{obs}, and for the corresponding theoretical values, giving the theoretical R-factor, R_{theo}. The black-body assumption for the stars in the IR region allows astronomers to use the Stefan-Boltzmann relation for the model integrated flux, σT_{eff}^4, in this method. This is given by (González Hernández & Bonifacio, 2009),

$$R_{\text{obs}} = \frac{F_{\text{bol}}(\text{Earth})}{F_{\lambda_{\text{IR}}}(\text{Earth})} = \frac{\sigma T_{\text{eff}}^4}{F_{\text{mod}}(\lambda_{\text{IR}}, T_{\text{eff}}, [\text{Fe/H}], \log g)} = R_{\text{theo}}. \tag{1.6}$$

$F_{\text{bol}}(\text{Earth})$ and $F_{\lambda_{\text{IR}}}(\text{Earth})$ both depend on the angular diameter, θ, of the star, which is cancelled in the R-factor. The $F_{\lambda_{\text{IR}}}(\text{Earth})$ is calculated using the absolute monochromatic flux and magnitude of a calibration star, the measured magnitude of the target star and a correction factor, which corrects for changes in the flux from the colour filters (González Hernández & Bonifacio, 2009).

The main disadvantages with the IRFM are that it is very dependent on reddening of the light, especially for stars further away from us, and that it is dependent on the measurements of the calibration star, for which Vega is often used. However, using Vega can cause considerable errors in the calculation as the magnitude and the flux can be difficult to measure with high enough accuracy. Accordingly, the method is sensitive to the accuracy in the data for the calibration star and hence also to which star is used (Casagrande et al., 2010).

1.4.2 Excitation balance

The effective temperature can also be determined based on the condition that the elemental abundance should be the same for several spectral lines with different excitation potentials (Ramírez et al., 2006). Fe I is the most common species to use since iron generates many spectral lines for FGK-type stars. If more lines are used, the precision of the method increases, which can be determined within 50 K accuracy. However, for metal-poor stars, too few iron lines are available, where other elements such as Ca, Ti or Si can be used instead (Jofré et al., 2019).

The main difficulties with this method is that it is sensitive to Non-Local Thermodynamic Equilibrium[1] (NLTE) and 3D effects. Especially Fe I lines are sensitive to NLTE effects, the main being overionization, which makes the calculated abundance more uncertain if assuming Local Thermodynamic Equilibrium (LTE) (Thévenin & Idiart, 1999). For lines formed in the deeper parts of the photosphere, the granulation have to be accounted for, which hence requires a 3D model when calculating the abundance.

In Bensby et al. (2014) they compare their results of the effective temperature calculated for LTE with NLTE. They only got differences of a few tens of K for F and G subgiant and dwarf stars, which is nearly negligible. However, they also discussed that 3D effects could have an impact on the results as well, but do not know which of the two effects dominates.

Lind et al. (2012) concluded that NLTE effects are not very significant in most giant stars. Only hot ($\gtrsim$ 5000 K depending on the surface gravity) or very metal-poor giants ($\lesssim -1$ dex depending on the surface gravity) show a clear impact in the determined temperature when comparing LTE and NLTE calculations. Otherwise, the difference between LTE and NLTE typically lies below ~ 50 K.

The NLTE and 3D effects most likely affect each other as well. In Asplund (2005) they discuss these effects and their impacts on different elements. They found that NLTE effects are greater in 3D than in 1D models in metal-poor stars due to their steep temperature structure. Their conclusion is that most likely both 3D and NLTE must be accounted for to get better results, especially for metal-poor stars. However, accounting for both NLTE and 3D effects complicates calculations and is therefore not widely used yet.

1.4.3 Balmer line profile fitting

Balmer lines are spectral lines formed from hydrogen transitions including the second energy level, $n = 2$. The line profiles of Balmer lines are very temperature sensitive. Thus, by comparing observed line profiles to synthetic, the temperature can be estimated.

Similarly as for the excitation balance, this method is sensitive to both NLTE and 3D effects in the stars. Convection is the main 3D effect that affects the profile of Balmer lines. An attempt to overcome this effect while still using 1D models in the synthetic Balmer lines is to add a factor called the mixing-length, a factor that takes the mixing of the gases from convection into account. However, it is shown that this is not enough to

---

[1] Radiative transfer dominates the energy transfer in the atmosphere and effects such as ionization are counted for, which complicates models and calculations.

fully reproduce the observed Balmer lines. In Ludwig et al. (2009) they explore the impact of using 3D instead of 1D modelling to reproduce the observed lines and discover that the mixing-length was not sufficient to correct for the differences in the synthetic lines. They conclude that a proper correction for the convection is required to acquire temperatures of desired accuracy, besides the mixing-length parameter.

NLTE effects generally affect the profiles of the Balmer lines less than the 3D effects do, since they often only affect the inner line wings and line cores because these are formed further out in the atmospheres where the collisions are less and therefore the NLTE effects are expected to be important. Likewise, since Hα, which is the transition between the levels $n = 2$ and $n = 3$, is formed in shallower layers of the stellar atmospheres, it is more sensitive to NLTE effects than the higher-order Balmer lines, hence negatively affecting the results. The lines also become more sensitive to NLTE effects in cooler stars as well as in metal-poor stars (Amarsi et al., 2018).

1.4.4 Interferometry

This method uses an interferometer to analyse stars' light by allowing the light to create an interference pattern. The pattern is then analysed to extract information about the stars. This way, the angular diameters of the stars can be determined as well as the bolometric flux from the stars (Karttunen et al., 2017). Limb-darkening describes the decrease in intensity of the light from stars' edges. This is caused by the decrease in temperature in shallower layers of the stars, which also causes weaker intensities. It is hence needed to determine a more accurate angular diameter of the stars, thus taking the decrease in intensity into account. The limb-darkened angular diameter, θ_{LD}, and the bolometric flux, F_{bol}, are then used in Equation 1.7 to get the effective temperature (Heiter et al., 2015),

$$T_{\mathrm{eff}} = \left(\frac{F_{\mathrm{bol}}}{\sigma}\right)^{0.25} (0.5\theta_{\mathrm{LD}})^{-0.5} . \tag{1.7}$$

Limb-darkening is very difficult to measure for stars that are small and far away. Therefore, the limb-darkened angular diameter, θ_{LD}, is the most difficult parameter to measure when determining the effective temperature. The limb-darkened angular diameter is easiest measured for nearby stars (Mozurkewich et al., 2003). Models are used to estimate the limb-darkening, which consequently provides errors to the angular diameters originating from the models (e.g. Karovicova et al. (2018)).

In Casagrande et al. (2014) it was also found that interferometry measurements become more difficult and uncertain for smaller stellar angular diameters, encouraging caution for stars with angular diameters smaller than 1 mas (milli-arcsecond).

Certain studies only determine the angular diameter through interferometry, while the bolometric flux is determined through other methods such as the IRFM. This limits the uncertainties caused by the interferometer to the angular diameter. Typical uncertainties when using this method are around 50 K, depending on the accuracy of the angular diameter and the bolometric flux (e.g. Karovicova et al. (2018)).

1.4.5 Spectral synthesis

The spectral synthesis method uses a program that creates synthetic spectra from given stellar parameters, which it then tries to fit to a measured spectrum. From this, the stellar parameters are estimated from the best possible fit to the spectrum.

Initially, codes calculated the equivalent widths for the spectral lines to estimate their abundances and from this, the appropriate effective temperature was determined to fit these abundances. It was for example used in Bensby et al. (2014) where they determined the iron abundance using equivalent widths after which they further used the iron abundance to determine other stellar parameters. However, using equivalent widths can cause overestimation of abundances if the spectral lines are blended, since the area of a single spectral line becomes more uncertain (Blanco-Cuaresma, 2019).

Synthetic spectra are used instead as they have the advantage of being able to handle line blending when fitting the spectra because they are not limited by the area of single spectral lines, which makes them superior to the equivalent-width method. However, both methods are dependent on which initial parameters and which spectral lines are used for the fits. Therefore, caution is recommended when choosing a method and associated parameters (Blanco-Cuaresma, 2019).

Several programmes have been created for this purpose. For example ATLAS/SYNTHE (Kurucz (1970)/Kurucz & Avrett (1981)), Moog (Sneden (1973)), MARCS/BACHUUS (initiated in Gustafsson et al. (1975)), SME (Valenti & Piskunov, 1996; Piskunov & Valenti, 2017), SPECTRUM (Gray & Corbally (1994)) and more. The program used in Jönsson et al. (in prep), from which the benchmark parameters for this thesis' stars are acquired from, is a code called Spectroscopy Made Easy (SME). It was also used in the third data release of the GALAH survey to analyse stellar spectra. Previously, SME had been used in a training set analysis for the second data release to test its capabilities and usefulness for this survey (Buder et al., 2021). SME synthesises spectra to fit specific, chosen spectral lines, instead of calculating the equivalent width.

1.5 Methods for determining $\log g$

Since the surface gravity is also important to understand stellar properties and spectra, several methods have been developed to measure this parameter. The main methods are discussed in the sections below where both the advantages and the disadvantages are explained.

1.5.1 Parallax

The method for determining the surface gravity through parallaxes is also called the trigonometric $\log g$ (Jofré et al., 2019). By combining the relations $g \propto \frac{M}{R^2}$ from Equation 1.3 and $L \propto R^2 T_{\text{eff}}^4$ from Equation 1.2, the surface gravity can be determined using the parallax through,

$$\log g = 0.4(V_0 + BC + 5\log\pi + 5 - M_{\mathrm{bol},\odot}) + \log g_\odot + 4\log\left(\frac{T_{\mathrm{eff}}}{T_{\mathrm{eff},\odot}}\right) + \log\left(\frac{M}{M_\odot}\right), \quad (1.8)$$

where V_0 is the apparent magnitude of the star, corrected for interstellar extinction, BC is the bolometric correction to the magnitude, π is the parallax in arcseconds (arcsec) and $M_{\mathrm{bol},\odot}$ is the Sun's bolometric magnitude (Nissen et al., 1997).

Parallaxes are dependent on the distance to the object under observation as the size of the parallax angle becomes smaller for larger distances. Accordingly, parallaxes become less accurate for stars at longer distances, which limits this method to closer stars. The uncertainties in the parallaxes also affects the determination of bolometric magnitudes, which causes more errors in the surface gravity (Jofré et al., 2019). It is also dependent on the mass, the effective temperature and magnitude measurements of the star. The mass alone can be complicated to determine as evolutionary tracks of stars are needed for this. It is restricted by the effective temperature, the stellar luminosity and the metallicity. Therefore, the uncertainty in the mass is affected by the uncertainties in these parameters, which furthermore affects the accuracy of the surface gravity (Heiter et al., 2015).

It is common to use the Hipparcos parallaxes in this method as they are very accurate. This typically gets uncertainties below 0.1 dex for the surface gravity. In addition, this method can be more extensively used since Gaia provides astronomers with accurate parallaxes for a larger stellar sample (Jofré et al., 2019). Gaia parallaxes are used in, for example, Buder et al. (2021) to determine the surface gravities of their stellar sample.

1.5.2 Ionization balance

Spectral lines are often more or less sensitive to the pressure in the atmosphere, which is affected by the surface gravity. The method of ionization balance aims to calculate the abundance of two ionization levels of a certain element, which should give the same abundance. For example, the abundance of iron should be the same no matter if one determines this quantity from Fe I lines or Fe II (singly ionized) lines (Jofré et al., 2019). Since the surface gravity affects the level of ionization for elements, with elements being differently sensitive to the effect, differently derived abundances can indicate the surface gravity of a star. Iron is the most commonly used element in this method as it has many spectral lines, especially in the optical region.

However, if there is not enough iron lines available for this method to give accurate results, other elements can be used as well. In Tsantaki et al. (2019) they used Ti lines to determine the surface gravity, which provided accurate results. They also discussed what they called the "ionization balance problem", which addresses that for several observed dwarf stars with a known surface gravity, the abundance derived from Fe I lines is not the same as derived from Fe II lines. This problem was also addressed in Mashonkina et al. (2011) where they concluded that this is probably caused by the determination of the effective temperature and/or problems in the stellar atmosphere modelling. However, the reason for this problem is yet unknown, but different ideas are discussed in this article. Their conclusion was that the main cause of the problem was that Fe II lines were often blended, causing inaccurate equivalent widths of the lines. By removing these blended lines, they limited the discrepancy in the abundances.

Another limitation of this method, when using iron lines, is that Fe II is more sensitive to the effective temperature of the star than neutral iron. Therefore, a small change in the temperature can change the strength of the Fe II lines while the Fe I lines remain more or less unaffected. Accordingly, the effective temperature of the star has to be accurately determined beforehand to get reliable results using this method (Tsantaki et al., 2019).

This method has uncertainties typically around 0.1 dex and is commonly used to determine the surface gravity spectroscopically. The main issue with this method, however, arises when there are not enough spectral lines to determine the surface gravity accurately (Jofré et al., 2019). This might occur in metal-poor stars as they do not have high enough abundances to create reliable spectral lines and too cool stars as they might not contain enough ionized elements.

1.5.3 Wings of strong lines

As was stated before, the wings of strong spectral lines are sensitive to the pressure within a star's atmosphere and are thus sensitive to broadening effects caused by the pressure. Accordingly, the wings are affected by the surface gravity of the star as well. By studying the wings of strong spectral lines, the surface gravity can be determined using stellar spectra. This can be done by fitting synthetic spectra to a measured one and from this, estimate the surface gravity. For this to be possible, the abundance of the element, whose lines are being used, must be determined through another method, such that the remaining parts of the wings are only dependent on the pressure. The effect of broadened, strong spectral lines is evident in FGK-type stars, which also makes this method useful for spectra with lower resolution. However, the sensitivity to the surface gravity in the spectral wings is generally not sensitive enough to detect very small changes in the surface gravity, which often limits the accuracy of this method (Jofré et al., 2019).

It is customary to often use strong metal lines for this method. In Fuhrmann et al. (1997) they used the Mg Ib lines (4571 and 5711 Å) to determine the surface gravity. They concluded that their results are reliable to 0.1 dex. Their main issue was that the metal-poor stars had few and weak spectral lines from metal elements, which increased the uncertainties for these stars. It made it difficult to determine the abundance due to the lack of lines and difficult to determine the surface gravity due to weak lines.

In Smith & Drake (1987) they used the Ca I 6162 Å line to determine the surface gravity. They got results with 0.1 dex accuracy. Again, the difficulty was to find strong enough lines that were sensitive to the surface gravity as many lines were too weak to be noticeably affected.

This method was also used in Jönsson et al. (2017) where they used Ca I lines. It was also used to determine the surface gravities for the benchmark parameters for this thesis' stellar sample.

1.5.4 Asteroseismology

Asteroseismology is the study of the oscillations of stars. Astronomers observe the pulsations and oscillations of stars and from this they interpret the frequency, amplitude and phase of the sound in the star. When looking at infrasound frequencies, astronomers can see deeper into the star's layers and thereby deduce how the layers are moving and what they look like (Aerts et al., 2010). Studying the frequency modes in a star's oscillations, the surface gravity can be directly determined. When knowing the effective temperature, the surface gravity can be determined to an accuracy of 0.01 dex when using this method (Jofré et al., 2019). In Morel & Miglio (2012) the results from using asteroseismology were compared to using ionization balance, pressure sensitivity in spectral line wings and isochrone modelling, when determining the surface gravity for the same stellar sample. In the survey, they used 40 bright stars that were either solar-like or red giant stars, where the maximum frequency power was well known. They concluded that the accuracy of the asteroseismology method was superior to the other methods, with uncertainties not exceeding 0.05 dex. The disadvantage of this method is that it is difficult to acquire results with good accuracy for metal-poor stars as they are faint (Jofré et al., 2019).

1.6 Summary

To summarize, IR spectroscopy is mainly beneficial because it is less affected by reddening and extinction. However, methods for spectral analysis of IR spectra are not fully developed due to technological difficulties that delayed the advancements. Important stellar properties are the effective temperature, the surface gravity and the metallicity. These can be measured through spectral analysis. Vibrational and rotational transitions dominate molecular spectra in the IR, which can be observed if the stars are cold enough such that the molecules do not dissociate. The effective temperature and the surface gravity can be determined through different methods where the majority use spectral analysis in some form, targeting different types of elements and spectral lines.

Since methods to determine effective temperatures in the IR are not developed yet, the purpose of this thesis is to provide insight into possible new methods by investigating if OH and CO lines can be used for this purpose. OH and CO spectral lines' sensitivities to the surface gravity, the oxygen abundance and the carbon abundance (for CO lines) are not fully explored either, which this thesis examines as well. The method is presented in the next chapter, where the tools and the procedure are explained.

Chapter 2

Method

In order to investigate the accuracy of determining the effective temperature from high resolution IR spectra of a set of K-giants, an exploration of the effective temperatures derived from molecular lines was done using synthetic spectral fitting. Therefore, the use of the spectral fitting is described in this chapter together with the program that was used. Information about the stellar sample, the model atmospheres and the line lists are also presented in the following sections.

The rest of the stellar input parameters are taken from Jönsson et al. (in prep). A few different line- and continuum-mask lists, see section 2.5, were used in SME to determine the temperatures, which were then compared to the known effective temperatures from Jönsson et al. (in prep). To determine the temperatures, a starting temperature was set to 4000 K for all measurements. The sensitivity of the surface gravity value in the stellar sample was examined by varying the known values with +0.2 and −0.2 dex (labeled $\log g_{\text{diff}}$) as this is a common uncertainty in determined surface gravities. Afterwards the oxygen abundance was varied similarly from the known values by +0.2 and −0.2 dex (labeled O_{diff}) to investigate the lines' sensitivity. Lastly, the CO lines' sensitivity to the carbon abundance was investigated as well by, again, varying the known values by +0.2 and −0.2 dex (labeled C_{diff}). Varying the oxygen abundance and the carbon abundance by ±0.2 dex as well, allowed for comparison between the different sensitivities.

2.1 Stellar Sample

34 K-giants were used in this thesis' stellar sample, which is a subset of the sample stars studied in Jönsson et al. (in prep). The stars have temperatures between 4000 and 5200 K, surface gravities between 1.3 and 3.3 dex and metallicities between -1.11 and 0.28 dex. Particularly K-giants were used because of the previously stated benefits. They were observed with IGRINS at the 4.3 m Lowell Discovery Telescope in Flagstaff, Arizona. The observations were done over the years 2019-2021 (PI: Ryde).

The stellar temperatures in Jönsson et al. (in prep), which are slightly updated compared to Jönsson et al. (2017), are considered good benchmark values as they agree with temperatures determined through angular diameters, which makes them considerably accurate. Therefore, they are good to compare the temperatures determined in this thesis to. The comparison between the temperatures makes it possible to estimate the accuracy and quality of the temperatures derived here.

Jönsson et al. (in prep) measured the spectra with the FIES spectrograph in the optical wavelength range. The observational differences are listed in Table 2.1 below. The temperatures were, however, determined in similar ways, through SME, which allows for a comparison between the different spectral lines used in the methods as well as using the optical versus the IR spectral range.

The stellar sample together with known stellar parameters from Jönsson et al. (in prep) are listed in Table A.1.

Table 2.1: Observational differences between Jönsson et al. (in prep) and this thesis.

Observational property	This Thesis	Jönsson et al. (in prep)
Spectrograph	IGRINS	FIES
Resolution	$45,000$	$67,000$
Wavelength range	$15,000$ - $18,000$ Å	3700 - 8300 Å

2.2 Line synthesis code

The temperatures were determined for the stars using a line synthesis method through a code named Spectroscopy Made Easy (SME). It was beneficial to use SME as the benchmark temperatures were determined with SME as well, thus removing potential uncertainties from using different programs. SME creates synthetic spectra based on a specific set of stellar parameters. The program uses the parameters to chose a suitable atmospheric model, which describes the temperature and pressure variations in the atmosphere, for the star of interest. The synthesised spectrum is then based upon calculations based on the model and known line data. Afterwards, the synthesized spectrum is compared to the observed spectrum, using a χ^2 minimization fitting routine. One or more of the initial parameters can also be set free. SME then creates several synthetic spectra based on different values of the free parameters, after which it choses the best matching spectra and provides the values of the determined free parameters. Another benefit of using SME is that it is capable of running batches of several stars at the same time (Valenti & Piskunov, 1996; Piskunov & Valenti, 2017), which saves time in the calculations.

Specific wavelength regions of the spectra are chosen for the χ^2 minimization. In these so-called segments the interesting lines to investigate are marked together with continuum regions. An example of such a segment is shown in Figure 2.1.

In this thesis, the effective temperature was set as a free parameter, from which it determined the temperature that generated the smallest χ^2. The surface gravity, $\log g$, the oxygen abundance, [O/Fe], and the carbon abundance, [C/Fe], were fixed in each iteration, but were varied between iterations with $\pm 0.2\,\text{dex}$ from the known values. The difference in the surface gravity, in the oxygen abundance and the carbon abundance were changed separately to determine the lines' sensitivity to the separate quantities.

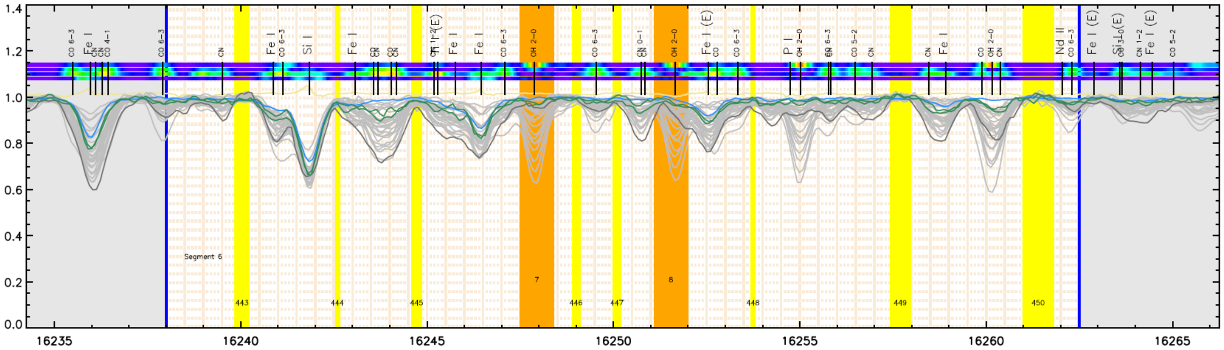

Figure 2.1: This figure shows an example of a small segment used in this thesis, where two OH lines are shown. The x-axis displays the wavelength in [Å] and the y-axis displays the continuum normalized flux. Continuum regions are marked with yellow, while line-regions are marked in orange. Several spectra can be seen in this segment as well: The light grey are all the spectra from the stellar sample, the blue is the Sun's spectrum and the dark grey spectrum is the spectrum of the metal-rich star μLeo. The bright yellow line shows the telluric spectrum, which is produced by molecules in the Earth's atmosphere. Since the spectra have been measured from Earth, the telluric spectrum has been divided out of the spectra such that telluric lines from the Earth's atmosphere do not affect the measurements. The telluric lines have been over plotted to indicate possible regions of the spectrum where the removal of the telluric lines might affect the quality of the observed spectrum. Lastly, a mainly blue line with colour variations can be seen above the spectra. This indicates where spectral lines are located and it is brighter where the lines are stronger.

2.3 Model Atmospheres

As was described in the previous section, SME uses model atmospheres when it synthesises spectra. For this thesis MARCS model atmospheres are used from Gustafsson et al. (2008). The MARCS models use several assumptions with the most important ones being:

- Spherical geometry. It is a more accurate approximation compared to the plane parallel geometry, which neglects for example limb-darkening because the photosphere normally makes up a very small part of the total stellar radius. For giants, however, plane parallel geometry does not work too well because the extension of the atmosphere is more significant. Spherical geometry takes this into account, which eliminates the problem.

- Hydrostatic equilibrium, which suggests that the photosphere is stable. It is therefore assumed that accelerations in the atmosphere are negligible compared to the surface gravity and that the mass-loss can be neglected as well. The hydrostatic equilibrium equation gives an approximation for the pressure structure in the atmosphere, where it is considered that the inner pressure and the gravity cancel each other out (Gray, 2021).

- Convection is modelled using mixing length theory. It approximates complicated 3D effects in the model into 1D.

- Local Thermodynamic Equilibrium (LTE), which is when collisional energy transfer is considered to dominate the energy distribution in the stellar atmosphere. LTE only holds for spectral lines formed in deeper layers of the photosphere, which means that it does not necessarily hold for strong lines. LTE does not always describe a stellar photosphere particularly well, especially in its shallower layers, but it still produces accurate enough results for this thesis (Gray, 2021).

2.4 Molecular Linelists

Linelists are lists containing information about spectral lines such as the wavelengths of the spectral line, the element notation together with its ionization state, its gf-value, which determines the probability of the transition (it is the statistical weight, g, times the oscillator strength, f) and broadening parameters of the line (for colder stars, such as K-giants, van der Waals broadening is particularly important). These lists are used by SME to identify the spectral lines used in the spectral synthesis.

The OH line list used in this thesis comes from Goldman et al. (1998), which extended the data for certain OH transitions from the HITRAN (HIgh-resolution TRANsmission) molecular spectroscopic database. As was explained in previous sections, weak lines are more reliable to use for analyses such as the one in this thesis and were hence used for the analysis. Blended lines were avoided as well to limit potential overestimation of the line strengths. The CO spectral line list comes from Goorvitch (1994), which provided a complete line list of ro-vibrational transitions for seven CO isotopes. The same properties of the spectral lines was targeted for the CO lines as was chosen for the OH lines.

2.5 Line- and continuum-masks

The χ^2 minimization regions were chosen to target the lines of interest in so-called line-mask lists. Lists with so-called continuum-masks show SME where it should try to normalize the spectra. Both line- and continuum-masks are included in different segments of the spectra. Together, these lists are included in the program as constraints to the line synthesis.

Three types of lists were used in this thesis: OH lines, CO lines and a combination of both OH and CO lines. The resulting temperatures for different values of $\log g_{\text{diff}}$ and $[\text{O/Fe}]_{\text{diff}}$ from each case is then compared with benchmark T_{eff} as well as with each other to see which works best for the temperature determination. It is also investigated if combining the spectral lines from both molecules will further improve the reliability of the determined temperatures. Lastly, $[\text{C/Fe}]_{\text{diff}}$ was changed for the CO linelists to compare the CO spectral lines' sensitivity to the carbon abundance, which furthermore was compared to its sensitivity to the oxygen abundance.

In the following chapter the results are presented and discussed, followed by conclusions.

Chapter 3

Results & Discussion

In this section the results are presented and discussed. This chapter is divided into four main parts: the first discusses the results when varying the surface gravity and the second discusses the results when varying the oxygen abundance. In each section different lines have been used (OH, CO or CO-OH combination), and they are discussed separately. The third discusses the results when varying the carbon abundance (for CO lines) and the fourth compares the three types of linemask lists.

The results are presented in multiple plots, displaying the difference between the effective temperature estimated in this thesis and the known effective temperatures from the benchmark, $\Delta T_{\rm eff}$, as a function of the benchmark temperatures. This way, the accuracy of this thesis' method is shown. In all the plots, the red, dashed lines mark the $\pm 100\,\mathrm{K}$ lines and the black line marks $\Delta T_{\rm eff} = 0\,\mathrm{K}$. Temperatures determined within the red, dashed lines ($\pm 100\,\mathrm{K}$) are considered good according to accuracy standards described for other methods used to determine the effective temperature.

For the OH lines there are two plots (Figure 3.2a and Figure 3.2b) displaying the same ratio as previously described with different colours representing the metallicity and the surface gravity of the stars, to see potential connections between both metallicity and determined temperatures, and the surface gravity and determined temperatures.

Lastly, plots displaying the linear regression fit to the difference between the determined $\Delta T_{\rm eff}$ for $\log g_{\rm diff}/\mathrm{O}_{\rm diff}/\mathrm{C}_{\rm diff} = 0.2\,\mathrm{dex}$ and $\log g_{\rm diff}/\mathrm{O}_{\rm diff}/\mathrm{C}_{\rm diff} = 0.0\,\mathrm{dex}$, are shown, where a relation between the change in surface gravity/oxygen abundance/carbon abundance and change in determined effective temperature can be estimated for this method.

3.1 Varying surface gravity

3.1.1 OH linelists

44 OH linemasks (approximately 50-60 lines) were used in the SME iterations, between $\sim$ 15180 Å and $\sim$ 16910 Å. These linemasks can be found in Table B.1 where their wavelength intervals, the number of lines within each mask and vibrational transitions are provided.

The OH lines used here have transitions between vibrational states with $\Delta\nu = 2$. Different lines with the same ν_{upper} and ν_{lower} are transitions between different rotational states within the vibrational states.

Figure 3.1a shows the accuracy of the determined effective temperature for the OH lines. All stars displayed in this plot lie within the ±100 K limit and show little difference in determined effective temperature between the various surface gravity values. The stars µLeo (4494 K), εVir (5112 K) and KIC6696436 (4520 K) deviated from the ±100 K lines and gave larger differences. It was concluded that εVir is too hot to contain any OH molecules and therefore lacks OH spectral lines, which made the fit poor and the determined temperature inaccurate. For giant stars, these lines are therefore recommended to be used for temperatures cooler than 5000 K. The other two stars had bad fits of the synthetic spectra (see an example in Figure C.1), which also produced poor temperatures. The reason for this is, however, unknown. Accordingly, these three stars were excluded from the analysis.

The linear regression made for the results is displayed in Figure 3.1b below, where it was fit to the difference in determined ΔT_{eff} between $\log g_{\text{diff}} = 0.2$ dex and $\log g_{\text{diff}} = 0.0$ dex. From this, it is concluded that a change of 0.2 dex in the surface gravity difference generates a change of approximately 1 K in the determined temperature. The OH spectral lines are thus not particularly sensitive to the surface gravity, which means that OH lines are useful to determine the effective temperature even if the determined surface gravity has larger uncertainties. OH lines' insensitivity to the surface gravity was also found in Decin et al. (2000), where they analysed how changing stellar parameters, such as the surface gravity, will affect the absorption by OH, CO, H_2O and SiO molecules in synthetic spectra of K- and M-giants.

It was also investigated if the OH lines' insensitivity to the surface gravity could be connected to the surface gravity or metallicity of the stars. In Figure 3.2a the same plot as in Figure 3.1a can be seen but the data points are coloured according to the respective metallicities. No relation can be found from this plot, which concludes that the stellar metallicity does not affect sensitivity of OH lines to changes in the surface gravity. Similar conclusions are made for the surface gravity as well, as it did not show any clear trend between the temperature difference and the known surface gravity. This can be seen in Figure 3.2b.

Figure 3.1

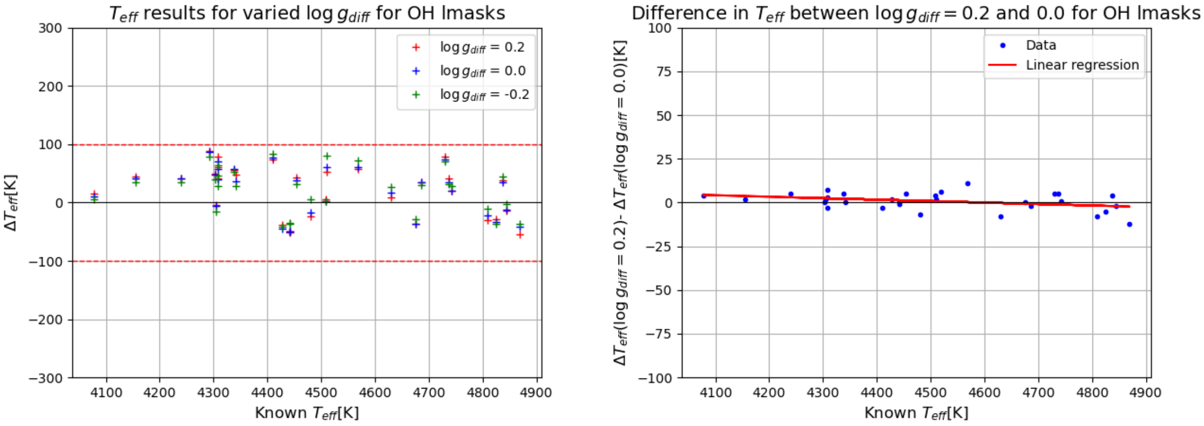

(a) The difference between the effective temperature determined in this thesis and the benchmark temperature displayed in [K] (y-axis). The benchmark temperature is shown in [K] (x-axis). The data points are marked with three different colours (red, blue and green), which represent $\log g_{\text{diff}}$: 0.2, 0.0 and −0.2 dex respectively.

(b) The difference between the T_{eff} difference for $\log g_{\text{diff}} = 0.2$ dex and the T_{eff} difference for $\log g_{\text{diff}} = 0.0$ dex in [K] (y-axis) as a function of the benchmark temperatures in [K] (x-axis). A linear regression fit to the above mentioned differences (marked in blue) is shown in red.

Figure 3.2

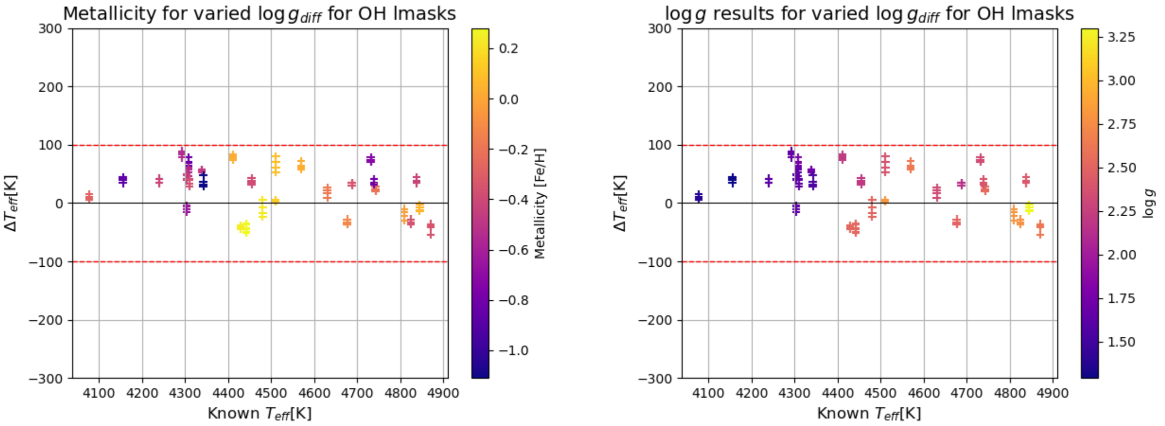

(a) The axes represent the same quantities as in Figure 3.1a. Different colours represent the metallicity (in dex) of the stars with corresponding colour bar shown to the right.

(b) The axes represent the same quantities as in Figure 3.1a. Different colours represent the surface gravity (in dex) of the stars with corresponding colour bar shown to the right.

3.1.2 CO linelists

26 linemasks containing approximately 100 CO lines were used in the SME iterations, within a span of ∼ 15570 Å to ∼ 16870 Å. The transitions were transitions between vibrational states with $\Delta\nu = 3$. Wavelength intervals, number of lines within each linemask and

vibrational transitions are presented in Table B.4.

In Figure 3.3a the accuracy of the determined effective temperatures from the CO lines is shown for various surface gravity values. The results are very spread out and almost half of the stars are outside the ±100 K lines. For the CO lines, only εVir (5112 K) deviates from the rest of the stars because it is too hot to contain any CO molecules, which produces a bad fit to the spectrum and hence less accuracy. It was therefore excluded from the analysis. Again, it is recommended to use these spectral lines if the giants are cooler than 5000 K.

The difference between the determined temperatures for the various surface gravity values is very large. According to the linear regression, which is displayed in Figure E.1, a change of 0.2 dex in the surface gravity gives a change of approximately 100 K in the determined temperature. This means that if CO lines are used to determine the effective temperature of a star, the determined surface gravity has to be very accurate to get reliable effective temperatures. Decin et al. (2000) also found that CO lines are sensitive to the surface gravity, further strengthening these results.

3.1.3 CO and OH combined linelists

A different set of OH linemasks was used for these SME iterations, which was shorter to save time. 17 linemasks, containing approximately 20 spectral lines, was used instead of 44 linemasks, as in subsection 3.1.1, because past experience suggests that using more lines does not improve the results significantly for this analysis. These linemasks lie within ∼ 15390 Å and ∼ 17110 Å, and are listed in Table B.3. The same CO linemasks that were used in the previous section was used in the combination as well.

Figure 3.3b shows the accuracy of using a combination of CO and OH spectral lines to determine the effective temperature. Most of the stars lie between the ±100 K lines and the difference between the determined effective temperatures for the various surface gravity values are fairly close. Three stars deviated from the results: μLeo (4494 K), εVir (5112 K) and HIP50583 (4292 K). These are the same stars that deviated for the OH linemasks in Table B.3, whose ΔT_{eff} results are presented in Figure D.1. This means that problems for the different spectral lines occur for the combination of the lines as well.

The linear regression in Figure E.2 shows that a change of 0.2 dex in the surface gravity gives a change of approximately -13 K in the determined temperature. Using the combination of the spectral lines therefore gives neither more accurate results, nor less sensitivity to surface gravity. The determined temperatures seem to get properties from both sets of spectral lines. The combination is less sensitive to the surface gravity than using purely CO lines, but it is not less sensitive than using purely OH lines.

Figure 3.3

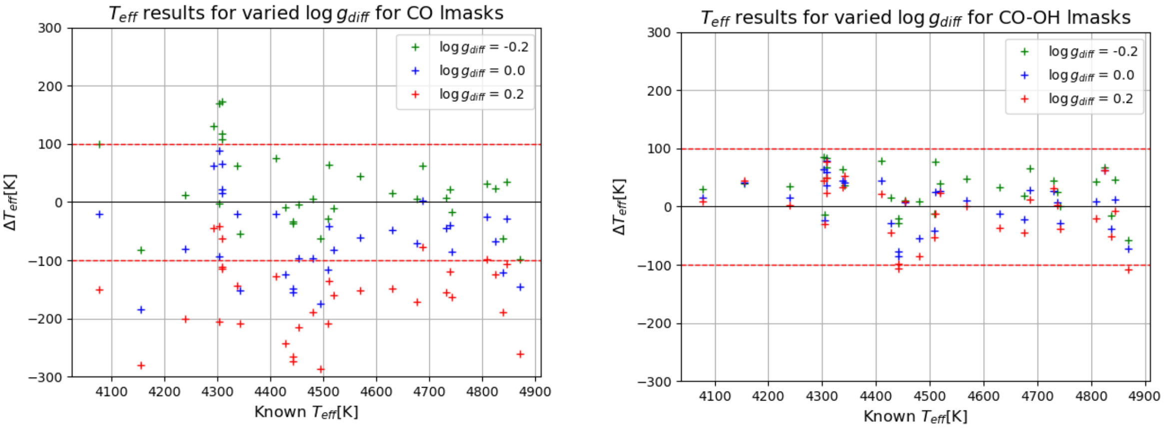

(a) The difference between the determined and the benchmark temperatures in [K] versus the benchmark in [K]. The data points are marked with three different colours (green, blue and red), which represent $\log g_{\text{diff}}$: -0.2, 0.0 and 0.2 dex respectively.

(b) The axes and the data points represent the same quantities as in Figure 3.3a but for the combined CO and OH linemasks.

3.2 Varying oxygen abundance

3.2.1 OH linelists

A shorter version of the linemasks that were used for the OH lines when varying the surface gravity difference, was used in the iterations here. OH lines within ~ 15230 Å and ~ 16910 Å were used with 30 linemasks containing a total of 37 spectral lines. These can be found in table Table B.2.

In Figure 3.4a the accuracy of the temperature determination for varying oxygen abundance can be seen. The results show that OH lines are very sensitive to the oxygen abundance, where the linear regression in Figure E.3 displays a change of approximately 120 K for a change of 0.2 dex in the oxygen abundance. Accordingly, the oxygen abundance have to be very accurate if one desires to use OH lines to determine the effective temperature.

Again, three stars in particular deviated from the rest: KIC6465057 (4825 K), KIC6837256 (4731 K) and HIP50583 (4292 K). Their determined temperatures were the same for all values of the oxygen abundance and according to the rest of the results, this should not be the case. It was found to be caused by a bug in the code, after which they were excluded from the analysis. Besides those three stars, εVir was excluded once again because of it lacking OH spectral lines.

Since the OH molecule is a diatomic molecule, it has a strong bond, hence a deep energy potential. However, it is not as strong as the CO molecule's bond. Accordingly, the OH molecules form from the oxygen left after forming CO molecules because of the stronger bonds. Thus, the OH abundance depends strongly on the oxygen abundance, which furthermore affects the determined effective temperature from the OH spectral lines.

Ryde et al. (2009) also found that changing the oxygen abundance affected the OH lines significantly.

3.2.2 CO linelists

The same linemasks that were used when varying the surface gravity were used for the CO lines here as well. Their results are displayed in Figure 3.4b. The majority of the stars are within the ±100 K lines and the difference between the determined temperatures is small for the various oxygen abundance values. εVir was excluded because of the lack of CO lines and the three stars KIC6465057 (4825 K), KIC6837256 (4731 K) and HIP50583 (4292 K) were excluded for the same reason as for the OH lines.

In Figure 3.5a the linear regression fit to the results similar to Figure 3.1b is displayed, which shows that a change of 0.2 dex in oxygen abundance changes the determined temperature by approximately 20 K. CO lines are therefore less sensitive to the oxygen abundance, which means that if CO lines are used to determine the temperature of stars, the oxygen abundance does not have to be very accurately known.

The CO molecule is a very strong molecule with a deep energy potential, which means that it has a large dissociation energy. Together with the fact that carbon is much less abundant than oxygen, the formation of CO molecules in stellar atmospheres consumes most oxygen needed to form as many CO molecules as possible. Therefore, the CO abundance only depends on the carbon abundance and not on the oxygen abundance as it takes all oxygen needed no matter the abundance. In Ryde et al. (2009) they found that the CO spectral lines were not significantly affected by the oxygen abundance, but that they were more affected by the carbon abundance.

Figure 3.4

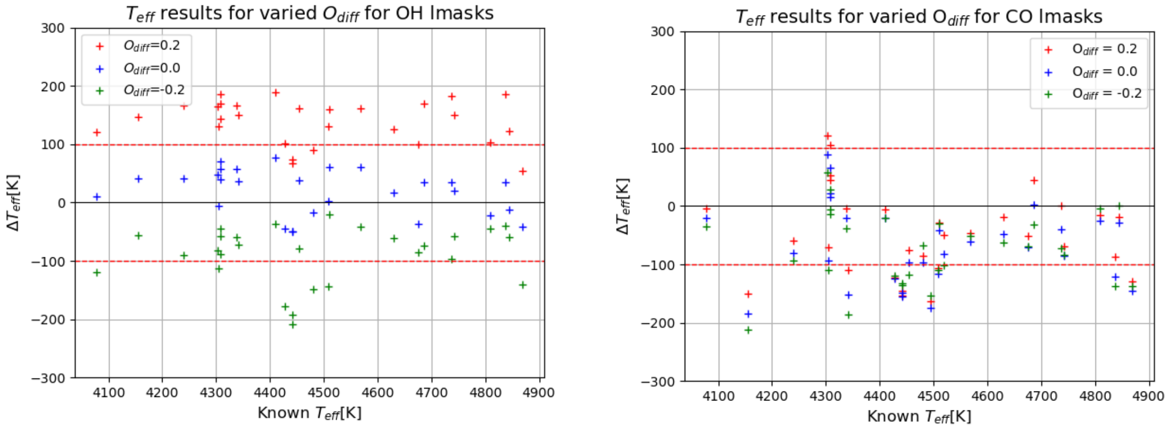

(a) The difference between the determined and the benchmark temperatures in [K] versus the benchmark in [K]. The data points are marked with three different colours (red, blue and green), which represent O_{diff}: 0.2, 0.0 and −0.2 dex respectively.

(b) The axes and the data points represent the same quantities as in Figure 3.4a but for CO linemasks.

3.2.3 CO and OH combined linelists

Figure 3.5b shows the accuracy in determined T_{eff} using a combination of the spectral lines for varying oxygen abundance. It shows a large sensitivity to the oxygen abundance, but less than the pure OH linemasks do. This again shows that the combination of the linemasks gets a combination of the properties of the separate linemasks.

The linear regression in Figure E.4 displays that the determined temperature changes with approximately 100 K for a change of 0.2 dex in the oxygen abundance. Accordingly, the combination of the spectral lines seems to be more affected by the oxygen lines' properties when determining the effective temperature in SME as the CO lines do not seem to dampen the oxygen abundance sensitivity. From the previous section, the sensitivity of the combination of linelists have similar sensitivity as the OH lines have as well. OH lines are therefore advised not to be used when the oxygen abundance is uncertain. A combination of OH and CO lines still present great sensitivity to the oxygen abundance and do not present accurate temperatures.

Figure 3.5

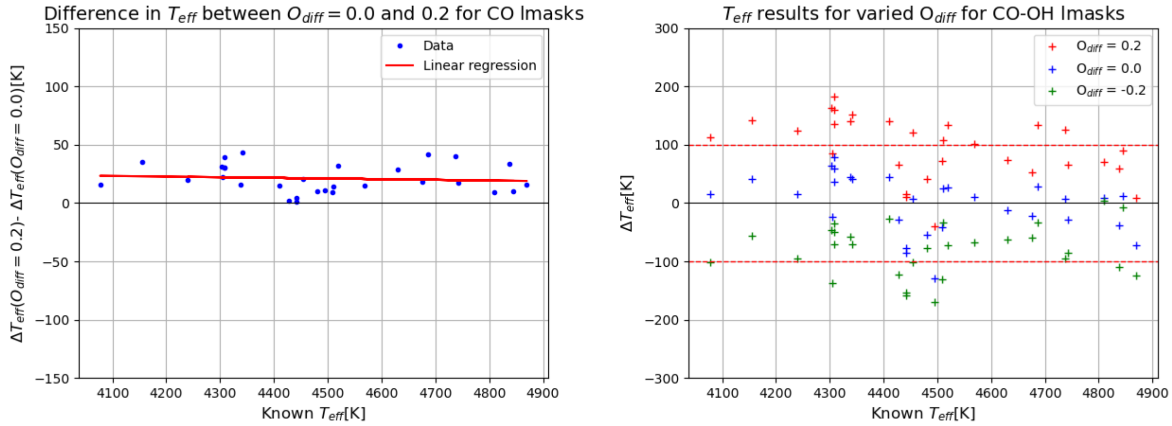

(a) The difference between the T_{eff} difference for $\mathrm{O_{diff}} = 0.2$ dex and the T_{eff} difference for $\mathrm{O_{diff}} = 0.0$ dex in [K] (y-axis) as a function of the benchmark temperatures in [K] (x-axis). A linear regression fit to the above mentioned differences (marked in blue) is shown in red.

(b) The difference between the determined and the benchmark temperatures in [K] versus the benchmark in [K]. The data points are marked with three different colours (red, blue and green), which represent $\mathrm{O_{diff}}$: 0.2, 0.0 and −0.2 dex respectively.

3.3 Varying carbon abundance

3.3.1 CO linelists

In Figure 3.6a the accuracy of the CO lines with varying carbon abundance is shown. It is clearly seen that the CO lines are very sensitive to the carbon abundance, where it shows a clear spread, with very few stars within the ±100 K limits. As before, εVir was excluded from the calculations. Otherwise, no stars deviated clearly from the group.

The linear regression fit to the difference between the ΔT_{eff}s for $\text{C}_{\text{diff}} = 0.2\,\text{dex}$ and $\text{C}_{\text{diff}} = 0.0\,\text{dex}$ is presented in Figure E.5. It shows that the determined effective temperature varies by $\sim 320\,\text{K}/0.2\,\text{dex}$ for the cooler stars, while it varies by $\sim 220\,\text{K}/0.2\,\text{dex}$ for the hotter stars. This clearly shows an improvement for higher temperatures where the difference in the carbon abundance affects the results less. However, even if there is an improvement, the difference is still large, and hence the lines are still very sensitive to the carbon abundance despite the higher temperatures. It is thus not more beneficial to use CO lines for hotter stars if the carbon abundance is inaccurate. Therefore, the carbon abundance must be very accurately known if CO lines are to be used in temperature determination of stars.

Similarly, as was described for the CO lines' sensitivities before, the abundance of CO molecules is strongly dependent on the amount of carbon in the star because it is much less abundant than the oxygen. The CO molecules are formed according to the amount of carbon available in the atmosphere, independently of the oxygen abundance. Hence, the CO lines are very sensitive to the carbon abundance, as is shown here and as was fund in Ryde et al. (2009) as well.

3.4 Comparison

In Figure 3.6b the differences between the determined temperatures and the benchmark temperatures for $\log g_{\text{diff}} = \text{O}_{\text{diff}} = \text{C}_{\text{diff}} = 0.0$ are shown for the OH linemasks, the CO linemasks and the combination linemasks. It shows that when using OH lines, the determined temperatures were roughly centred slightly above $\Delta T_{\text{eff}} = 0\,\text{K}$, while the CO lines were centred below $\Delta T_{\text{eff}} = 0\,\text{K}$ in the plot. The combination of the two is centred in between the different lines, around the $\Delta T_{\text{eff}} = 0\,\text{K}$ line. It therefore seems like the CO lines drag down the determined temperatures and get them closer to the truth or known T_{eff}s. This again shows the combined properties that the combination linemasks get from using both sets of linelists.

Figure 3.6

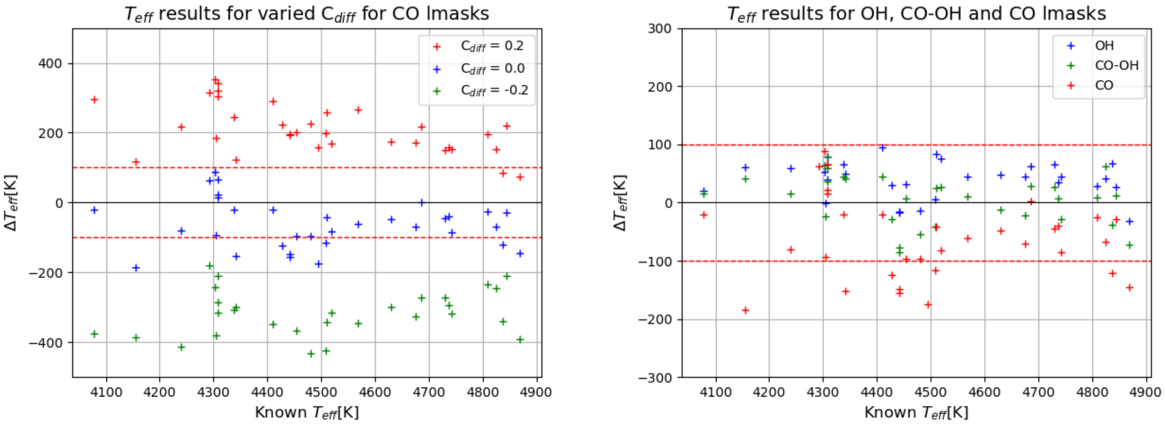

(a) The difference between the determined and the benchmark temperatures in [K] versus the benchmark in [K]. The data points are marked with three different colours (red, blue and green), which represent C$_{\text{diff}}$: 0.2, 0.0 and -0.2 dex respectively. Note that the y-axis has a different limit compared to the previous plots (± 500 K).

(b) The difference between the determined and the benchmark temperatures in [K] versus the benchmark in [K] for the T_{eff} results for $\log g_{\text{diff}} = \text{O}_{\text{diff}} = 0.0$ dex. The data points are marked with three different colours (blue, green and red), which represent the linelists: OH, CO-OH combination and CO respectively.

Chapter 4

Conclusion

To conclude, star spectra are a treasure trove of information that helps us learn more about the Milky Way and its evolution and history. Effective temperature is one of the most important fundamental stellar parameters as it is directly related to the energy output of the star and because it affects the spectral lines as well. Methods for determining the effective temperature in stars from IR spectra are not fully developed, because technological difficulties to create reliable IR detectors have delayed the development of these methods. It is, however, beneficial to observe in the IR since it does not get obscured by interstellar dust and is hence not sensitive to reddening either.

The majority of the methods used to determine effective temperatures, except for the IRFM, use the optical wavelength range in the analysis and they use different properties of spectral lines to determine the temperature. When using the best equipment for observation, they all have uncertainties below 100 K, but they all have disadvantages as well. For example, NLTE and 3D effects can decrease the accuracy of Balmer line profile fitting and excitation balance, and interferometry is sensitive to how accurate the determined angular diameter of the star is.

In this thesis it is explored if the effective temperature can be determined in the IR by fitting synthetic spectra using SME to OH and CO spectral lines. The OH and the CO molecules are both temperature sensitive and provide numerous spectral lines originating from ro-vibrational transitions in the IR spectral range. Their potential sensitivities to the surface gravity, the oxygen abundance and the carbon abundance (for CO lines) are explored as well.

It was found that OH lines provide accurate temperatures within ±100 K accuracy, which are insensitive to the surface gravity but very sensitive to the oxygen abundance. CO lines were discovered to provide less accurate temperatures but the majority of the determined temperatures are still within ±100 K, but generally underestimate the temperatures. They are very sensitive to the surface gravity and the carbon abundance but less sensitive to the oxygen abundance. The combination of the OH and CO lines provided accurate temperatures, mainly in between the determined temperatures from the separate linelists. It also acquired properties from both sets of linelists, minimising the sensitivities of the lines when combined. They, however, seem to get more properties from the OH lines' sensitivities, such as lower sensitivity to the surface gravity but larger sensitivity to the oxygen abundance.

The spectral lines from both molecules become very weak when the giant star is too hot. Therefore, these lines are recommended to be used for giants below $\sim 5000\,\mathrm{K}$. When the surface gravity is uncertain, OH lines are best to be used to determine the effective temperature and the combination of the lines is beneficial to use as well since it is found to be insensitive to the surface gravity. Conversely, CO lines are best to be used when the oxygen abundance is uncertain and the surface gravity is certain and the combination is best used when the OH lines' sensitivity to the oxygen abundance needs to be minimised. If the carbon abundance is uncertain, CO lines should not be used at all, since this provides unreliable results. In that case, it is best to use OH lines alone.

Even if many conclusions were found in this thesis' measurements, there is still many things left to explore. It might, for example, be interesting to investigate the combination of the lines further and in particular investigate if it is general that the combination acquires more properties from the OH lines than from the CO lines. Then it might be interesting to potentially find why this is and what causes it. Does the amount of lines from the two molecules affect this and might the choice of the lines affect the results as well? Another set of measurements that could be interesting to explore is to set the effective temperature, the surface gravity and the oxygen abundance free and see how this affects the determined effective temperatures and maybe also see if the determined surface gravities and oxygen abundances are accurate or very different from the known values.

Bibliography

Aerts, C., Christensen-Dalsgaard, J., & Kurtz, D. W. 2010, Asteroseismology., Astronomy and Astrophysics Library (Springer Netherlands)

Amarsi, A. M., Nordlander, T., Barklem, P. S., et al. 2018, A&A, 615, A139

Asplund, M. 2005, Annual Review of Astronomy and Astrophysics, 43, 481

Bensby, T., Feltzing, S., & Oey, M. S. 2014, A&A, 562, A71

Blackwell, D. E. & Shallis, M. J. 1977, MNRAS, 180, 177

Blanco-Cuaresma, S. 2019, MNRAS, 486, 2075

Buder, S., Sharma, S., Kos, J., et al. 2021, MNRAS, 506, 150

Buyana, T. 1997, Molecular physics. [Electronic resourse]. (World Scientific)

Casagrande, L., Portinari, L., & Flynn, C. 2006, MNRAS, 373, 13

Casagrande, L., Portinari, L., Glass, I. S., et al. 2014, MNRAS, 439, 2060

Casagrande, L., Ramírez, I., Meléndez, J., Bessell, M., & Asplund, M. 2010, A&A, 512, A54

Decin, L., Waelkens, C., Eriksson, K., et al. 2000, A&A, 364, 137

Fuhrmann, K., Pfeiffer, M., Frank, C., Reetz, J., & Gehren, T. 1997, A&A, 323, 909

Goldman, A., Schoenfeld, W., Goorvitch, D., et al. 1998, Journal of Quantitative Spectroscopy and Radiative Transfer, 59, 453, atmospheric Spectroscopy Applications 96

González Hernández, J. I. & Bonifacio, P. 2009, A&A, 497, 497

Goorvitch, D. 1994, Astrophysical Journal Supplement, 95, 535

Gray, D. F. 2021, The Observation and Analysis of Stellar Photospheres (Cambridge: Cambridge University Press)

Gray, R. O. & Corbally, C. J. 1994, AJ, 107, 742

Gustafsson, B., Bell, R. A., Eriksson, K., & Nordlund, A. 1975, A&A, 42, 407

Gustafsson, B., Edvardsson, B., Eriksson, K., et al. 2008, A&A, 486, 951

Heiter, U., Jofré, P., Gustafsson, B., et al. 2015, A&A, 582, A49

Jofré, P., Heiter, U., & Soubiran, C. 2019, Annual Review of Astronomy and Astrophysics, 57, 571

Jönsson, H., Ryde, N., Nordlander, T., et al. 2017, A&A, 598, A100

Karovicova, I., White, T. R., Nordlander, T., et al. 2018, MNRAS, 475, L81

Karttunen, H., Kröger, P., Oja, H., Poutanen, M., & Donner, K. J. 2017, Fundamental Astronomy. (Springer Berlin Heidelberg)

Kurucz, R. L. 1970, SAO Special Report, 309

Kurucz, R. L. & Avrett, E. H. 1981, SAO Special Report, 391

Lind, K., Bergemann, M., & Asplund, M. 2012, MNRAS, 427, 50

Ludwig, H. G., Behara, N. T., Steffen, M., & Bonifacio, P. 2009, A&A, 502, L1

Mashonkina, L., Gehren, T., Shi, J. R., Korn, A. J., & Grupp, F. 2011, A&A, 528, A87

Masseron, T. 2015, in SF2A-2015: Proceedings of the Annual meeting of the French Society of Astronomy and Astrophysics, 303–305

Morel, T. & Miglio, A. 2012, Monthly Notices of the Royal Astronomical Society: Letters, 419, L34

Mozurkewich, D., Armstrong, J. T., Hindsley, R. B., et al. 2003, AJ, 126, 2502

Nissen, P. E., Hoeg, E., & Schuster, W. J. 1997, in ESA Special Publication, Vol. 402, Hipparcos - Venice '97, ed. R. M. Bonnet, E. Høg, P. L. Bernacca, L. Emiliani, A. Blaauw, C. Turon, J. Kovalevsky, L. Lindegren, H. Hassan, M. Bouffard, B. Strim, D. Heger, M. A. C. Perryman, & L. Woltjer, 225–230

Piskunov, N. & Valenti, J. A. 2017, A&A, 597, A16

Ramírez, I., Allende Prieto, C., Redfield, S., & Lambert, D. L. 2006, A&A, 459, 613

Rieke, G. H. 2009, Experimental Astronomy, 25, 125

Ryde, N., Edvardsson, B., Gustafsson, B., et al. 2009, A&A, 496, 701

Short, C. I. & Bennett, P. D. 2021, Publications of the Astronomical Society of the Pacific, 133, 064501

Smith, G. & Drake, J. J. 1987, A&A, 181, 103

Smith, V. V., Cunha, K., Shetrone, M. D., et al. 2013, ApJ, 765, 16

Sneden, C. A. 1973, Phd thesis, University of Texas at Austin

Storey, J. W. V. 2000, Publications of the Astronomical Society of Australia, 17, 270–274

Thévenin, F. & Idiart, T. P. 1999, ApJ, 521, 753

Tsantaki, M., Santos, N. C., Sousa, S. G., et al. 2019, MNRAS, 485, 2772

Valenti, J. A. & Piskunov, N. E. 1996, in Astronomical Society of the Pacific Conference Series, Vol. 108, M.A.S.S., Model Atmospheres and Spectrum Synthesis, ed. S. J. Adelman, F. Kupka, & W. W. Weiss, 175

Watkins, M., Jerram, P., Pratlong, J., & Gil-Otero, R. 2020, in X-Ray, Optical, and Infrared Detectors for Astronomy IX, ed. A. D. Holland & J. Beletic, Vol. 11454, International Society for Optics and Photonics (SPIE), 1 – 18

Yuk, I.-S., Jaffe, D. T., Barnes, S., et al. 2010, in Ground-based and Airborne Instrumentation for Astronomy III, ed. I. S. McLean, S. K. Ramsay, & H. Takami, Vol. 7735, International Society for Optics and Photonics (SPIE), 653 – 662

Appendix A

Stellar sample

Table A.1: Stars used in this thesis together with their temperatures, surface gravities, metallicities, oxygen abundances and carbon abundances.

Star names	$T_{\rm eff}$[K]	$\log g$[dex]	[Fe/H]	[O/Fe]	[C/Fe]
αBoo	4308	1.66	-0.55	0.62	0.18
µLeo	4494	2.51	0.27	-0.05	-0.03
HD102328	4442	2.52	0.28	0.03	0.03
HD102338_K3III	4442	2.52	0.28	0.03	0.33
εVir	5112	3.01	0.11	0.03	-0.25
βGem	4809	2.81	-0.02	0.08	-0.16
HIP50583	4292	1.65	-0.54	0.32	-0.06
HIP63432	4155	1.29	-0.87	0.57	0.00
HIP72012	4077	1.38	-0.28	0.20	-0.05
HIP90344	4454	2.20	-0.39	0.38	0.03
HIP96014	4240	1.62	-0.43	0.25	0.07
HIP102488	4742	2.53	-0.21	0.24	-0.08
2M17215666	4342	1.55	-1.11	0.70	-0.02
KIC3748585	4569	2.63	0.03	0.14	-0.08
KIC3955590	4411	2.21	0.03	0.20	0.06
KIC4177025	4309	1.65	-0.37	0.50	0.4
KIC4659706	4428	2.52	0.24	0.13	0.08
KIC5113910	4338	1.72	-0.48	0.28	-0.04
KIC5709564	4687	2.15	-0.35	0.50	0.14
KIC5779724	4303	1.63	-0.45	0.53	0.24
KIC5859492	4511	2.38	0.09	0.13	-0.01
KIC5900096	4480	2.51	0.23	0.05	0.05
KIC6465075	4825	2.78	-0.37	0.26	-0.08
KIC6547007	4738	2.39	-0.81	0.57	0.19

Table A.1: Stars used in this thesis together with their temperatures, surface gravities, metallicities, oxygen abundances and carbon abundances. Continued from table on previous page.

Star names	T_{eff}[K]	$\log g$[dex]	[Fe/H]	[O/Fe]	[C/Fe]
KIC6696436	4520	2.19	-0.40	0.28	-0.03
KIC6837256	4731	2.33	-0.73	0.58	0.14
KIC10186608	4676	2.50	-0.12	0.15	-0.05
KIC11045542	4304	1.64	-0.65	0.27	0.02
KIC11342694	4509	2.82	0.14	0.03	-0.03
KIC11444313	4630	2.33	-0.18	0.17	0.00
KIC11569659	4838	2.42	-0.43	0.39	0.02
KIC11657684	4870	2.62	-0.35	0.26	-0.07
2M14231899+050079	4308	1.77	-0.82	0.77	0.25
HD142091_K0III	4845	3.30	0.06	0.14	-0.06

Appendix B

Used linemasks

B.1 OH lines

Table B.1: The long linemask list used for the OH linelist in this thesis. For information about the specific spectral lines within the linemasks, check the linelist provided by Goldman et al. (1998).

Wavelength interval [Å]	# of lines	Vibrational transition ($\nu_{\mathrm{upper}} - \nu_{\mathrm{lower}}$)
15182.25 - 15183.65	2	3 - 1
15236.00 - 15237.50	2	3 - 1
15277.70 - 15279.30	1	2 - 0
15280.30 - 15281.70	1	2 - 0
15390.20 - 15392.00	2	3 - 1
15406.00 - 15408.00	1	2 - 0
15408.40 - 15409.70	1	2 - 0
15421.65 - 15423.05	1	2 - 0
15433.50 - 15435.50	1	4 - 2
15469.20 - 15470.70	1	4 - 2
15504.70 - 15506.70	2	3 - 1
15559.65 - 15561.10	1	2 - 0
15568.00 - 15569.50	1	2 - 0
15571.40 - 15573.00	1	2 - 0
15625.85 - 15628.10	2	3 - 1
15651.15 - 15654.50	1	3 - 1
15716.45 - 15717.80	1	2 - 0
15719.00 - 15720.50	1	2 - 0
15725.70 - 15727.40	1	2 - 0

Table B.1: The long linemask list used for the OH linelist in this thesis. For information about the specific spectral lines within the linemasks, check the linelist provided by Goldman et al. (1998). Continued table from previous page.

Wavelength interval [Å]	# of lines	Vibrational transition ($\nu_{\text{upper}} - \nu_{\text{lower}}$)
15729.20 - 15731.20	1	2 - 0
15754.90 - 15757.10	2	3 - 1
16061.00 - 16063.00	1	2 - 0
16064.20 - 16065.80	1	2 - 0
16068.80 - 16070.35	1	2 - 0
16247.20 - 16248.80	1	2 - 0
16254.30 - 16256.00	1	2 - 0
16259.40 - 16260.80	1	2 - 0
16274.70 - 16275.80	2	5 - 3
16311.80 - 16313.55	2	4 - 2
16345.60 - 16348.00	2	4 - 2
16351.35 - 16252.80	1	3 - 1
16354.00 - 16355.20	1	3 - 1
16367.60 - 16368.55	1	3 - 1
16525.60 - 16526.90	1	3 - 1
16534.00 - 16535.30	1	3 - 1
16580.50 - 16583.00	2	4 - 2
16604.10 - 16606.00	1	4 - 2
16713.70 - 16715.05	1	3 - 1
16871.10 - 16872.80	2	2 - 0
16885.30 - 16887.00	1	4 - 2
16894.70 - 16896.30	1	3 - 1
16898.30 - 16899.75	1	3 - 1
16901.60 - 16903.40	1	4 - 2
16908.60 - 16910.20	1	3 - 1

Table B.2: A short version of the previous linemask list in Table B.1 used for the OH linelist when changing O_{diff} in this thesis. For information about the specific spectral lines within the linemasks, check the linelist provided by Goldman et al. (1998).

Wavelength interval [Å]	# of lines	Vibrational transition ($\nu_{upper} - \nu_{lower}$)
15236.00 - 15237.50	2	3 - 1
15277.70 - 15279.30	1	2 - 0
15280.30 - 15281.70	1	2 - 0
15390.20 - 15392.00	2	3 - 1
15406.00 - 15408.00	1	2 - 0
15408.40 - 15409.70	1	2 - 0
15504.70 - 15506.70	2	3 - 1
15568.00 - 15569.50	1	2 - 0
15571.40 - 15573.00	1	2 - 0
15625.85 - 15628.10	2	3 - 1
15651.15 - 15652.40	1	3 - 1
15716.45 - 15717.80	1	2 - 0
15719.00 - 15720.50	1	2 - 0
15754.90 - 15757.10	2	3 - 1
16064.20 - 16065.80	1	2 - 0
16247.20 - 16248.80	1	2 - 0
16254.30 - 16256.00	1	2 - 0
16259.40 - 16260.80	1	2 - 0
16311.80 - 16313.55	2	4 - 2
16351.35 - 16252.80	1	3 - 1
16354.00 - 16355.20	1	3 - 1
16367.60 - 16368.55	1	3 - 1
16525.60 - 16526.90	1	3 - 1
16534.00 - 16535.30	1	3 - 1
16604.10 - 16606.00	1	4 - 2
16713.70 - 16715.05	1	3 - 1
16871.10 - 16872.80	2	2 - 0
16885.30 - 16887.00	1	4 - 2
16894.70 - 16896.30	1	3 - 1
16908.60 - 16910.20	1	3 - 1

Table B.3: The short linemask list used for the OH linelist when combining the CO and OH linelists in this thesis. For information about the specific spectral lines within the linemasks, check the linelist provided by Goldman et al. (1998).

Wavelength interval [Å]	# of lines	Vibrational transition ($\nu_{\mathrm{upper}} - \nu_{\mathrm{lower}}$)
15390.70 - 15391.70	2	3 - 1
15406.60 - 15408.00	1	2 - 0
15568.00 - 15569.50	1	2 - 0
15651.45 - 15652.35	1	3 - 1
15730.00 - 15731.00	1	2 - 0
15754.80 - 15757.20	2	3 - 1
16052.30 - 16053.50	1	3 - 1
16247.50 - 16248.40	1	2 - 0
16251.10 - 16252.00	1	2 - 0
16367.70 - 16368.80	1	3 - 1
16447.60 - 16448.60	1	2 - 0
16525.80 - 16526.90	1	3 - 1
16604.80 - 16606.00	1	4 - 2
16713.70 - 16715.15	1	3 - 1
16908.50 - 16909.90	1	3 - 1
17099.25 - 17100.90	3	2 - 0
17104.24 - 17105.20	1	3 - 1

B.2 CO lines

Table B.4: The long linemask list used for the CO linelist in this thesis. For information about the specific spectral lines within the linemasks, check the linelist provided by Goorvitch (1994). The transitions marked with * represent transitions based on linelist energies.

Wavelength interval [Å]	# of lines	Vibrational transition ($\nu_{\text{upper}} - \nu_{\text{lower}}$)
15577.00 - 15583.75	14	3 - 0
15600.40 - 15601.10	1	3 - 0
15774.60 - 15776.10	4	4 - 1*
15779.50 - 15782.50	4	4 - 1
15783.30 - 15784.40	2	4 - 1
15785.50 - 15786.80	2	4 - 1
15982.70 - 15984.20	2	5 - 2
15984.60 - 15986.50	2	5 - 2
15986.90 - 15993.70	6	5 - 2
15995.30 - 15996.80	2	5 - 2
15998.90 - 16001.50	3	5 - 2, 3 - 0
16010.50 - 16012.50	2	5 - 2
16186.75 - 16189.80	5	5 - 2*, 3 - 0*
16399.40 - 16402.20	4	7 - 4*
16402.80 - 16404.10	2	7 - 4*
16410.70 - 16411.70	2	7 - 4*
16413.80 - 16414.70	2	7 - 4*
16420.70 - 16422.00	2	7 - 4
16613.00 - 16618.80	12	8 - 5*/7 - 4*
16625.50 - 16627.80	4	8 - 5, 7 - 4*
16628.60 - 16630.80	3	8 - 5, 7 - 4
16640.00 - 16641.70	2	8 - 5
16643.50 - 16645.00	2	8 - 5*, 7 - 4
16834.70 - 16837.40	7	8 - 5*
16848.30 - 16850.10	2	9 - 6
16859.65 - 16864.70	7	9 - 6, 8 - 5, 5 - 2*

Appendix C

Bad fit

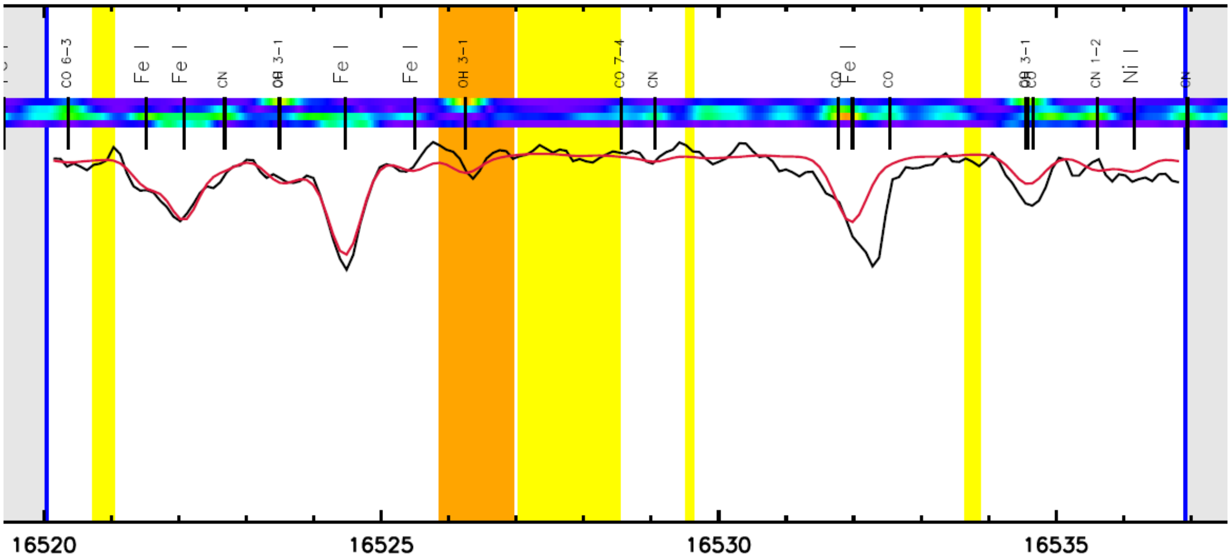

Figure C.1: A segment of the fitted synthetic spectrum (red) and the observed spectrum (black) for the star KIC6696436 for $\log g_{\mathrm{diff}} = \mathrm{O}_{\mathrm{diff}} = \mathrm{C}_{\mathrm{diff}} = 0.0\,\mathrm{dex}$, when using OH linemasks.

Appendix D

OH result for extra linemasks

Figure D.1 shows the ΔT_{eff} results for the OH linemasks presented in Table B.3, which are the same linemasks used for the CO-OH combination. For this set of linemasks, three stars deviated from the ±100 K lines. Namely, µLeo (4494 K), εVir (5112 K) and HIP50583 (4292 K).

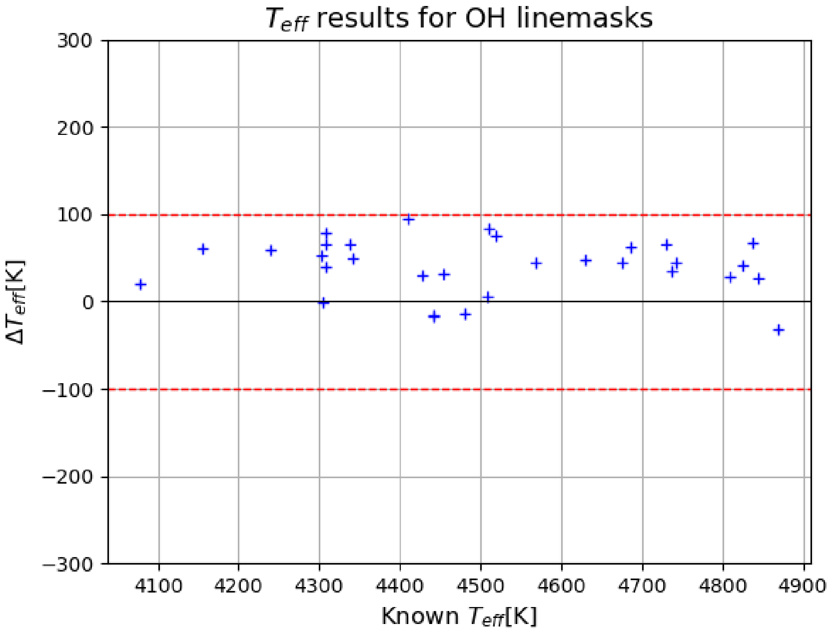

Figure D.1: The difference between the determined and the benchmark temperatures in [K] versus the benchmark in [K]. The data points are marked blue, which represent $\log g_{\text{diff}} = 0.0\,\text{dex}$.

Appendix E

Linear regressions

E.1 Changing surface gravity

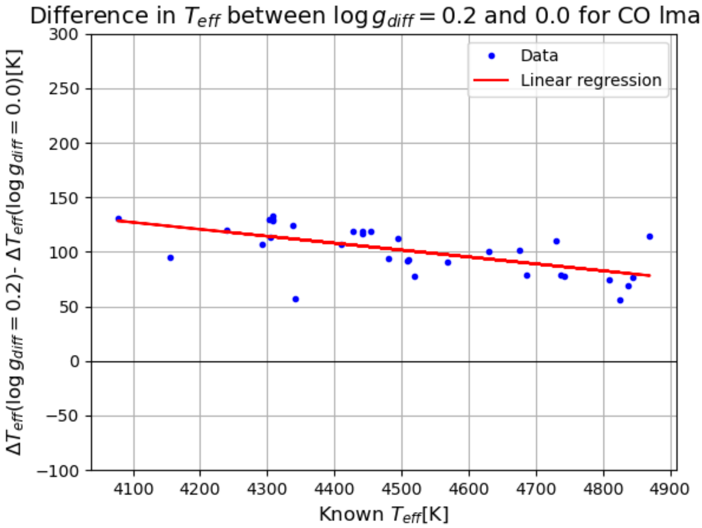

Figure E.1: The difference between the $T_{\rm eff}$ difference for $\log g_{\rm diff} = 0.2\,$dex and the $T_{\rm eff}$ difference for $\log g_{\rm diff} = 0.0\,$dex in [K] (y-axis) as a function of the benchmark temperatures in [K] (x-axis). A linear regression fit to the above mentioned differences (marked in blue) is shown in red.

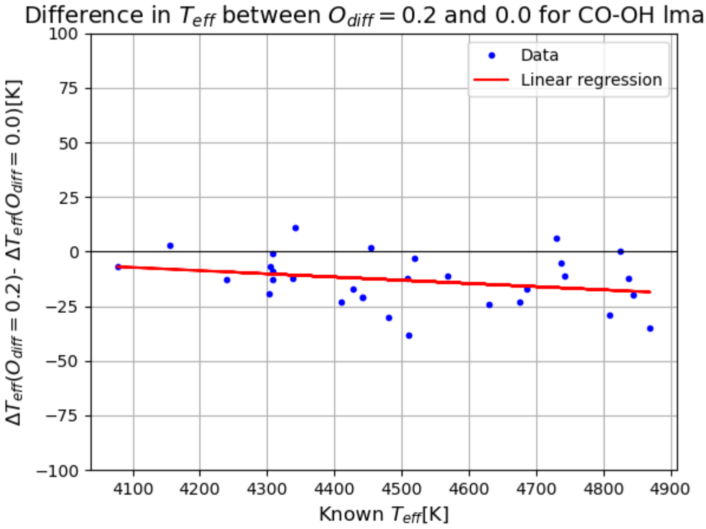

Figure E.2: The difference between the $T_{\rm eff}$ difference for $\log g_{\rm diff} = 0.2$ dex and the $T_{\rm eff}$ difference for $\log g_{\rm diff} = 0.0$ dex in [K] (y-axis) as a function of the benchmark temperatures in [K] (x-axis). A linear regression fit to the above mentioned differences (marked in blue) is shown in red.

E.2 Changing oxygen abundance

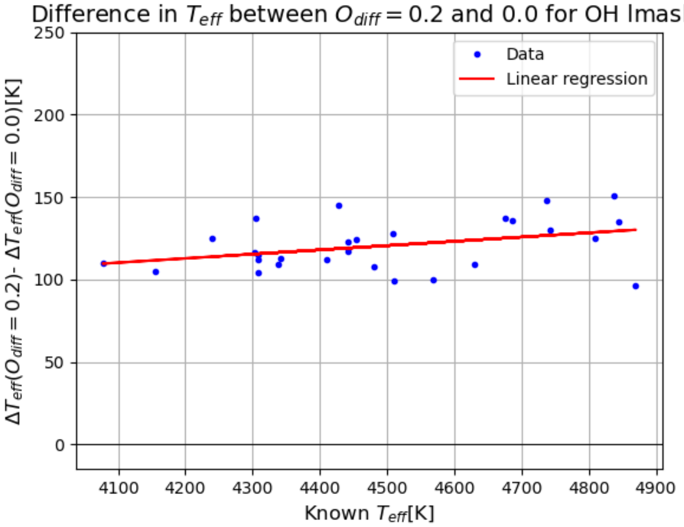

Figure E.3: The difference between the $T_{\rm eff}$ difference for $\rm O_{diff} = 0.2$ dex and the $T_{\rm eff}$ difference for $\rm O_{diff} = 0.0$ dex in [K] (y-axis) as a function of the benchmark temperatures in [K] (x-axis). A linear regression fit to the above mentioned differences (marked in blue) is shown in red.

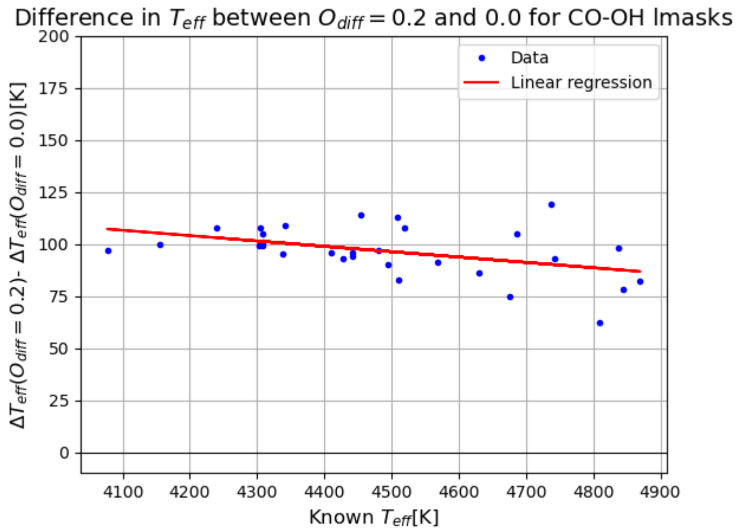

Figure E.4: The difference between the T_{eff} difference for $\text{O}_{\text{diff}} = 0.2$ dex and the T_{eff} difference for $\text{O}_{\text{diff}} = 0.0$ dex in [K] (y-axis) as a function of the benchmark temperatures in [K] (x-axis). A linear regression fit to the above mentioned differences (marked in blue) is shown in red.

E.3 Changing carbon abundance

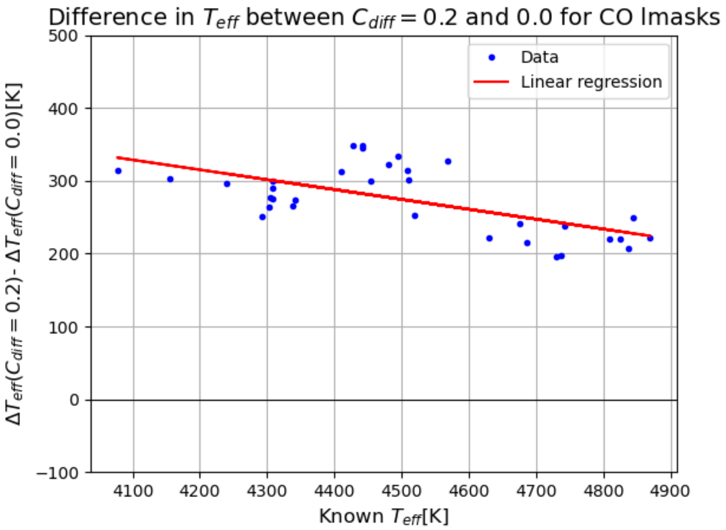

Figure E.5: The difference between the T_{eff} difference for $\text{C}_{\text{diff}} = 0.2$ dex and the T_{eff} difference for $\text{C}_{\text{diff}} = 0.0$ dex in [K] (y-axis) as a function of the benchmark temperatures in [K] (x-axis). A linear regression fit to the above mentioned differences (marked in blue) is shown in red.